

A Thesis

entitled

Verification and Validation Method for  
an Acoustic Mode Prediction Code for Turbomachinery Noise

by

Jeffrey Severino

Submitted to the Graduate Faculty as partial fulfillment of the requirements for the  
Masters of Science Degree in Mechanical Engineering

---

Dr. Ray Hixon, Committee Chair

---

Dr. Chinhua Sheng, Committee Member

---

Dr. Soric Cioc, Committee Member

---

Dr. Patricia R. Komuniecki, Dean  
College of Graduate Studies

The University of Toledo

- 2022

Copyright 2022, Jeffrey Severino

This document is copyrighted material. Under copyright law, no parts of this document may be reproduced without the expressed permission of the author.

An Abstract of  
Verification and Validation Method for  
an Acoustic Mode Prediction Code for Turbomachinery Noise

by  
Jeffrey Severino

Submitted to the Graduate Faculty as partial fulfillment of the requirements for the  
Masters of Science Degree in Mechanical Engineering

The University of Toledo  
- 2022

Over the last 20 years, there has been an increase in computational fluid dynamic codes that have made numerical analysis more and more readily available, allowing turbomachine designers to create more novel designs. However, as airport noise limitations become more restrictive over time, reducing aircraft takeoff and landing noise remains a prominent issue in the aviation community. One popular method to reduce aircraft noise is using acoustic liners placed on the walls of the engine inlet and exhaust ducts. These liners are designed to reduce the amplitude of acoustic modes emanating from the bypass fan as they propagate through the engine. The SWIRL code is a frequency-domain linearized Euler equation solver that is designed to predict the effect of acoustic liners on acoustic modes propagating in realistic sheared and swirling mean flows, guiding the design of more efficient liner configurations. The purpose of this study is to validate SWIRL using the Method Of Manufactured Solutions (MMS). This study also investigated the effect of the integration and spatial differencing methods on the convergence for a given Manufactured Solution. In addition, the effect of boundary condition implementation was tested. The improved MMS convergence rates shown for these tests suggest that the revised SWIRL code provides more accurate solutions with less computational effort than the original formulation.

# Acknowledgments

This work is supported by the NASA Advanced Air Transport Technologies (AATT) Project. I would like to thank Edmane Envia of the NASA Glenn Research Center, who is the technical monitor of this work. A very special thanks goes to Dr. Ray Hixon who supervised and guided me through out my course work and Master's Thesis. His rigor and tenacity in his profession has been the model example for an aspiring aeroacoustician. I would like to also thank all of my committee members, Dr. Chunhua Sheng and Dr. Sorin Cioc. Their contributions have been instrumental. Thanks to Dr. Clifford Brown for his programatic insights.

I would also like to thank my focus group peers, Zaid Sabri, Matthew Gibbons , and Gabriel Gutierrez for their patience and support over the years. I wish them the best in all of their endeavours.

# Contents

<b>Abstract</b>	<b>iii</b>
<b>Acknowledgments</b>	<b>iv</b>
<b>Contents</b>	<b>v</b>
<b>List of Tables</b>	<b>viii</b>
<b>List of Figures</b>	<b>ix</b>
<b>List of Symbols</b>	<b>xi</b>
<b>List of Abbreviations</b>	<b>xiii</b>
<b>Preface</b>	<b>xiv</b>
<b>1 Introduction</b>	<b>1</b>
1.1 Overview . . . . .	1
<b>2 Literature Review</b>	<b>7</b>
2.1 Introduction . . . . .	7
2.1.1 The problem to be addressed and its significance . . . . .	7
2.1.2 Establish reasoning - i.e. point - of - view for reviewing the literature . . . . .	7
2.1.3 Explain the order/sequence of the review . . . . .	9
2.1.4 The theoretical foundation of conceptual framework . . . . .	10

2.2	Golubev and Atassi's work . . . . .	11
2.3	Review of the assessment of the numerical techniques . . . . .	12
2.3.1	The research questions, hypotheses, foreshadowed problems, or conjectures . . . . .	13
2.3.2	Calculation of Observed Order-of-Accuracy . . . . .	15
2.4	Conclusion . . . . .	18
<b>3</b>	<b>Theoretical Framework and Methods</b>	<b>19</b>
3.1	Introduction . . . . .	19
3.2	Governing Equations for Compressible, Inviscid Flow . . . . .	19
3.3	Nonuniformities from swirling mean flow . . . . .	21
3.4	Linearizing the Governing Equations . . . . .	22
3.5	Non-Dimensionalization . . . . .	24
<b>4</b>	<b>Verification and Validation Techniques for Numerical Approxima- tions</b>	<b>28</b>
4.1	Introduction . . . . .	28
4.1.1	Examining Convergence Using Multiple Grids . . . . .	30
4.1.2	Calculation of Observed Order-of-Accuracy . . . . .	31
4.2	Methods . . . . .	34
4.2.1	Procedure . . . . .	35
4.2.2	Tanh Summaion Formulation . . . . .	36
4.3	General form of a Hyperbolic Tangent . . . . .	36
4.4	Setting Boundary Condition Values Using a Fairing Function . . . . .	42
4.4.1	Using $\beta$ as a scaling parameter . . . . .	42
4.4.2	Minimum Boundary Fairing Function . . . . .	44
4.4.3	Max boundary polynomial . . . . .	46
4.4.4	Corrected function . . . . .	46

4.4.5	Symbolic Sanity Checks . . . . .	47
4.4.6	Min boundary derivative polynomial . . . . .	48
4.4.7	Polynomial function, max boundary derivative . . . . .	49
4.4.8	Putting it together . . . . .	51
<b>5</b>	<b>Results and Discussion</b>	<b>52</b>
5.1	Verification of Numerical Schemes using the Method of Manufactured Solution . . . . .	52
5.1.1	Introduction . . . . .	52
5.1.2	MMS, Solutions . . . . .	53
	<b>References</b>	<b>66</b>

# List of Tables



# List of Figures

1-1	The evolution of the directivity and the relative levels of sources as a function of engine architecture (a)low bypass-ratio (b) high bypass ratio [34]	2
5-1	The manufactured mean flow test case using a summation of Tangents for $A$ and $M_x$	54
5-2	A comparison of the speed of sound, expected vs actual at the lowest grid to show similarities in solution	55
5-3	A comparison of the speed of sound error at three grid	56
5-4	L2 Norm comparison for the speed of sound integration for the compound trapezoidal rule	56
5-5	The manufactured perturbation functions $,v_r$	57
5-6	The manufactured perturbation functions $,v_x$	58
5-7	The manufactured perturbation functions $,v_\theta$	58
5-8	The manufactured perturbation functions $,P$	59
5-9	Speed of Sound Rate Of Convergence	60
5-10	Comparison of manufactured source term for the first linearized Euler equation	60
5-11	Comparison of manufactured source term for the second linearized Euler equation	61
5-12	Comparison of manufactured source term for the third linearized Euler equation	61

5-13 Comparison of manufactured source term for the fourth linearized Euler equation . . . . .	62
5-14 LEE Source Term Error . . . . .	62
5-15 LEE Source Term Error . . . . .	63
5-16 LEE Source Term Error . . . . .	63
5-17 LEE Source Term Error . . . . .	64

# List of Symbols

$A$ .....	mean flow speed of sound
$A_T$ .....	speed of sound at the duct radius
$\tilde{A}$ .....	dimensionless speed of sound, $\frac{A}{A_T}$
$D/Dt$ .....	material derivative, $\partial/\partial t + V \cdot \nabla$
$D_N$ .....	derivative matrix using $N$ points
$\mathbf{e}_x, \mathbf{e}_\theta$ .....	unit vectors for the axial and tangential directions
$k_x$ .....	perturbation axial wavenumber
$k$ .....	reduced frequency, $\omega r_{max}/A_T$
$m$ .....	number of nodal diameters, i.e. azimuthal mode number
$M_x$ .....	axial Mach number
$M_\theta$ .....	tangential Mach number
$P$ .....	mean pressure
$p'$ .....	perturbation pressure
$r$ .....	radial coordinate
$r_{min}$ .....	hub radius, i.e. minimum radius
$r_{max}$ .....	hub radius, i.e. maximum radius
$\bar{r}$ .....	dimensionless radial coordinate, $r/r_{max}$
$\bar{r}_{Shankar}$ .....	dimensionless radial coordinate in ?? , $r/b = r/(r_{max} - r_{min})$
$S$ .....	mean entropy
$s'$ .....	perturbation entropy
$t$ .....	time
$\vec{V}$ .....	mean flow velocity vector
$v$ .....	mean flow velocity
$v'$ .....	perturbation flow velocity
$v_x$ .....	axial component of mean flow velocity
$v_\theta$ .....	tangential component of mean flow velocity
$v'_r$ .....	axial component of perturbation velocity
$v'_x$ .....	axial component of perturbation velocity
$v'_\theta$ .....	tangential component of perturbation flow velocity
$v_\phi$ .....	phase velocity, $k/\bar{\gamma}$
$v_g$ .....	group velocity, $dk/d\bar{\gamma}$
$x$ .....	axial coordinate

### *Greek Symbols*

$\bar{\gamma}$ .....	dimensionless axial wavenumber, $k_x r_{max}$
$\Gamma$ .....	free vortex strength
$\bar{\Gamma}$ .....	$\Gamma/(r_T A_T)$
$\delta$ .....	Kronecker delta
$\eta_H$ .....	hub acoustic liner admittance (at $r_{min}$ )
$\eta_T$ .....	tip acoustic liner admittance (at $r_{max}$ )
$\Theta$ .....	circumferential/azimuthal coordinate
$\kappa$ .....	ratio of specific heats
$\kappa_{m\mu}$ .....	modal separation constant
$\lambda$ .....	eigenvalue, $-i\bar{\gamma}$
$\mu$ .....	radial mode index
$\bar{\rho}$ .....	mean density
$\rho'$ .....	perturbation density
$\sigma$ .....	hub-to-tip radius ratio, $r_{min}/r_{max}$
$\Omega$ .....	angular frequency for solid body swirl
$\bar{\Omega}$ .....	$\Omega r_T/A_T$
$\omega$ .....	perturbation angular frequency

# List of Abbreviations

CAA .....	Computational Aeroacoustics
CFD .....	Computational Fluid Dynamics
MMS .....	Method of Manufactured Solutions
TSM .....	Tanh Summation Method
NS .....	Navier-Stokes
RK .....	Runge-Kutta

# Preface

# Chapter 1

## Introduction

### 1.1 Overview

Since the dawn of commercial airlines in the early 20th century, the increased demand for aircraft transport introduced jet engines to support large cargo and passengers. Consequently, this rise in innovation resulted in high volume engine noise due to the frequency of flights. After 1975, efforts to reduce aircraft noise eliminated the noise pollution for 90% of the population [4]. However, given the rapid increase in aircraft movements and consequently increase in noise exposure to larger populations, the advancement in noise reduction technologies has only been moderately increasing, leaving a requirement for in aeroacoustic modeling techniques and treatment strategies to compete with the demand for quiet subsonic flight [3]. Between the 1950s and 1960's jet engine designs shifted to higher bypass ratios with two or three shafts. The high bypass ratio (HBP) fan utilized multiple stages of fans and air streams [34]. The efficiency of these engines rose with the availability of materials that are able to cool flows passing over the turbofan, thus slowing the overall jet velocity but maintaining the efficiency of the engine. Due to the increase in high-bypass-ratio of turbomachines, the newest models of engines have a significantly larger diameter and a shorter nacelle, leaving less room to place acoustic treatments in regions where it

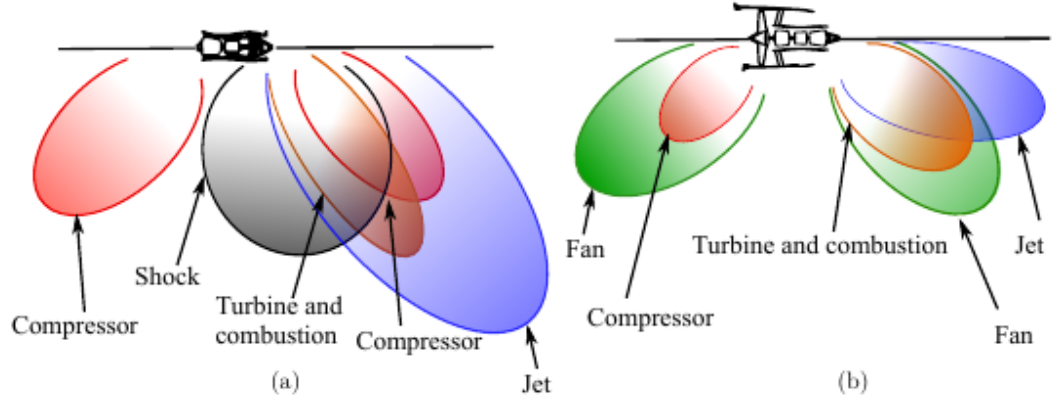


Figure 1-1: The evolution of the directivity and the relative levels of sources as a function of engine architecture (a) low bypass-ratio (b) high bypass ratio [34]

will be effective [27]. Figure 1-1 shows the evolution of directivity for turbomachines as the use of HBR fans became more popular. As these engines continue to develop, an increased understanding of sound propagation within the interstage of the engine is going to be needed due to flow behavior (high compressibility and rotational effects). While a turbomachine's general flow condition includes a series of axial, tangential, and radial velocity components that vary depending on the location of concern, the swirling flow between fan stages has been an area of interest due to the potential for acoustic treatment in a location previously avoided for its flow complexity. This work will explore how sound propagation is modeled and how the current state of code verification and validation (V&V) currently stands. This introduction will describe how fluid mechanics is utilized to establish an aeroacoustic model for various ducted flows. It will also discuss how code verification is used in the computational and numerical fields but will show the need for the use of these code verification techniques for a frequency domain CAA code.

In general, jet engine designers can model flow within a turbomachine with the Navier Stokes (N-S) Equations, a set of partial differential equations that describe



the mass, momentum and energy of a given viscous fluid, however these equations can be computationally expensive as they are used in the most general cases.

For aeroacousticians, the N-S equations can be used to identify sound generation and propagation because acoustic waves are low amplitude ( only a fraction of atmospheric pressure) and are not strongly influenced by viscosity.

As a result, it is common in practice to utilize the Linearized Euler equations (LEE), a closely related set of PDEs that model inviscid fluid, as they provide an approximation for higher Reynold number flows where viscosity does not play a critical role. Each to modeling sound propagation within a flow is to “linearize” the Euler equations, which decomposes the flow solution into a mean and fluctuating component . The decomposition is done in a linear fashion because the sound propagation amplitude is small with respect to the mean flow, and their presence does not appreciable change the mean flow field. The flow solution’s decomposition gives rise to linear and nonlinear terms in the Euler equations where the non-linear fluctuating components are neglected.

The LEE provides a system of linear equations where the solution is a family of wavenumbers and radial mode shapes that arise from unsteady disturbances for flows within a cylindrical duct. Another method decomposes the flow into vortical and potential parts [15]. In either case, this presents an initial value problem which in limited cases can obtain analytical solutions for simplified mean flow. Once a mean flow is contains a tangential component, the LEE equations must be solved numerically. For uniform flows in a hard wall duct , the waves are categorized as vortical ,entropic, and acoustic waves. The vortical and entropic waves solely convect with the mean flow, where as the acoustic wave can propagate without damping or decay exponentially. However, for swirling flows, the waves are partially coupled and are not easily categorized due to an additional category of “nearly convecting” modes [23],[22] . Therefore, the families of waves must be found numerically [10] making the

ducted acoustic propagation in swirling flow a problem without an analytical solution but has a framework for a numerical solution. Swirling flow has been a difficult problem to investigate in comparison to flows parallel to the wall domain of a duct [9] because of the lack of an analytical solution and thus cannot be described from a single convective wave equation. However, the solution for sheared mean flows was first presented by Goldstein [11],[12]. Various special cases of swirling flow (free vortex and solid body swirl) was examined in [21] [23], [22]. In recent years V & V has been done given the rise in technologies capable of experimentally measuring the acoustic modes within a turbomachine [28]. This work aims offer additional insight to the V & V process by expanding on techniques used in this field.

Computational codes are widely used in the field of aeroacoustics and concerted effort has recently been made to improve V & V techniques by Ingraham and Hixon [20, 19]. The question of getting the correct answer was a large focus of this work.

This thesis aims to continue this effort by conducting code verification and validation on a frequency domain Linearized Euler equation approximation on previous work done by Pratt & Whitney and NASA Glenn Research Center through technical contract [25, 26].

The algorithms presented in this thesis have been written using FORTRAN 77 and has been updated to FORTRAN 90, and implemented into a code named SWIRL. The foundational work has been started by Pratt and Whitney by Kenneth Kousen [25] and continued by Dr. Ray Hixon. SWIRL analyzes axial flows with mean shear and swirl in hard wall and acoustically lined ducts. The Method of Manufactured Solutions (MMS) is a process for generating an analytical solution for a code that provides the numerical solution for a given domain. The goal of MMS is to establish a manufactured solution that can be used to establish the accuracy of the code within question. For this study, SWIRL, a code used to calculate the radial modes within an infinitely long duct is being validated through code verification. SWIRL accepts a

given mean flow and uses numerical integration to obtain the speed of sound. The integration technique is found to be the composite trapezoidal rule through asymptotic error analysis.

Prior work has largely depended on conducting code validation through exact solutions to the partial differential equation (PDE) , the convective wave equation . Such a procedure formally known as the method of exact solutions (MES) [2]. MES has the advantage in that the output of SWIRL can be directly compared to the solution of the PDE, however available solutions are limited for sound propagation in ducted flows.

The literature review in the next chapter will discuss the governing equations that are used to predict the acoustic behavior in a fluid flowing internally, followed by the research problem that arises in swirling flow, the objectives and questions, the significance and finally the limitations. The proposed research aims to determine the impact of the numerical schemes used in the swirling flow problem and how it effects the family of waves that are produced from the problem formulation so a better understanding of the acoustic phenomena as the flow under goes a compressible rotational flow. The use of the method of manufactured solutions is used as a means of ensuring the code is correctly approximating the governing equations and will check the effect of the numerical schemes on the axial wavenumbers produced.

The use of numerical approximations are powerful for cases where there is no analytical solution, thus leaving multiple ways of arriving at a numerical solution. The use of MMS allows the user to obtain various metrics such as the approximated asymptotic rate of convergence, or the grid convergence index, to identify if the code is performing as intended , i.e. using the right equations.

The goal of this research is to conduct component level code verification tests for the problem of characterizing the duct acoustics for flow using a LEE model by looking at the two numerical components for SWIRL.

The goal of The proposed component verification from Kleb and Wood will be presented to address the characterization of modes and the presence of numerical ones.

Hypothesis. further improve the result.

# Chapter 2

## Literature Review

### 2.1 Introduction

#### 2.1.1 The problem to be addressed and its significance

The impact of swirling flow has been , there has been a concerted effort to model sound propagation under such conditions. This has lead to a number of publications that attempt to discern the acoustic signature of swirling flow through a cylindrical domain [23] , [22], [25], [26], [15] ,[13],[14], [35], [29], [16], [9], [8], [30], [17].

#### 2.1.2 Establish reasoning - i.e. point - of - view for reviewing the literature

A large amount of aircraft noise was reduced from 1975-2000, effectively eliminating the noise pollution for 90% of the population [4]. Since the early 2000's, the advancement in noise reduction technologies has been gradual, leaving a requirement for drastic improvement in aeroacoustic treatment strategies to compete with the demand of quiet subsonic flight. A previous theoretical review by Envia has been suggested that a non linear time domain computation could capture the source gener-

ation (incident turbulence) in addition to the broadband noise. Such a process would have the capabilities of solving all components of noise generation in an individual calculation [10]. This would at minimum, require an “LES-type” fidelity code, which can tend to be computationally expensive. A promising option is NASA GRC’s Broadband Aeroacoustic Stator Simulation (BASS). BASS is a high-order, high accuracy computational aeroacoustics (CAA) code which has been used to study non linear provides mean an extensive study of non linear phenomena in turbomachinery flow, and in particular, mechanisms of noise generation that are produced from unsteady disturbances. This code allows for a wide variety of finite differencing and time marching schemes as well as artificial dissipation methods. This effective computational tool allows for an in-depth modeling of realistic velocity profiles that would be representative of flow produced from a rotor blade row. In recent work, a new method of implementing realistic, three-dimensional rotor wakes free from acoustics was validated [18]. This provides a means of studying acoustic responses non linear swirling flows within pragmatic geometric configurations, while simultaneously allow for the modeling of sources generation produced from the incident turbulence.

Over the last 40 years, several studies have investigated the impact of swirling flow on the sound propagation with the use of the 3D linearized Euler equations, directly solving the unsteady equations as opposed to approximating the solutions to both steady and unsteady flow problems. Another NASA code, LINFLUX predict acoustic disturbances from blade movements in subsonic flows. While LINFLUX demonstrates capabilities to model three dimensional steady and unsteady flows, the computational time is larger compared to lower fidelity codes that only compute the unsteady portion of the problem. The benefit of such a code is beneficial to engine and liner designers who are interested in a wide range of configurations, requiring a parametric study. SWIRL [26], is a code that conducts an eigenmode analysis by assuming a constant radius annular or cylindrical duct with acoustically lined walls

using the linearized unsteady Euler equations. Such a code is needed to identify the modal content and can be used as a boundary condition with LINFLUX by using a mode matching technique. The goal of this theoretical review is to see the current state of low-fidelity frequency domain LEE codes and where the foundational model differs depending on the problem formulation.

### **2.1.3 Explain the order/sequence of the review**

This review will compare studies that have considered the applicability of unsteady linearized Euler equations on cylindrical and annular ducts. First the work of Kousen will be briefly summarized [26, 25]. Secondly, the alternate approach shown by Golubev and Atassi used in [13, 14] were also compared. These works have utilized a standard normal mode approach to determine the modal response of inviscid, compressible, swirling flow within a cylindrical and annular ducts. Results and findings have revealed three categories of associated wave - modes, acoustic, nearly convected, and nearly sonic. Detailed examination of the literature indicate that the hierarchical system was not initially apparent. A qualitative description of the numerical methods used to evaluate the eigensystem of solutions will be described. The use of the Method of Manufactured Solutions will also be described. While its use is widespread in the verification and validation community, very little aeroacoustic codes utilize the MMS to apply code verification. This review will discuss the procedures and guidelines associated with the MMS, and some specific measures that were taken to ensure that the guidelines were met and that the suggestions used in literature were expanded upon.

#### 2.1.4 The theoretical foundation of conceptual framework

One key question that remains, is how well do unsteady linearized equations capture the mechanisms of noise generation within realistic turbomachinery flow? There exists a copious amount of published work describing the use of wave equations to describe the governing behavior of ducted sound propagation. However, turbomachines inherently rely on high velocities, high temperatures to maximize efficiencies. Such mechanisms need a more thorough formulation so that a complete acoustic description of the flow can be provided.

To begin exploring various geometries, we must first ask: what are the central theories that have been used to explain the acoustic behavior of unsteady swirling flows? Do the linearized Euler equations provide an adequate means of capturing the mechanisms of noise generation within realistic turbomachinery flow? The study was expanded by [22, 38] who included cases of solid body swirl. Wundrow studied the swirling potential flows using Goldstein’s disturbance velocity decomposition [11] using a numerical approach and found that the solutions were more accurate and found more efficiently [22]. Kousen expanded these efforts by including [25, 26] the effect unsteady disturbances in the presence of forced solid body-swirl and free-vortex flow without the use of potential flow theory. Using normal mode analysis along with a radial spatial differencing scheme, the wave modes produced within cylindrical and annular ducts was reported. Results show (figure 4.7) two distinct families of modes, purely convected and acoustic modes. The presence of axial shear in combination solid body flows can endue coupling between these modes, which in theory would not appear unless viscous terms were present in the eigenvalue analysis. Lack of available swirl flow results “hampered” validation attempts. However, this eigenvalue approach was utilized with a new quasi-3D formulation to find the axial wavenumbers from solid body flow was proposed in his next work .



In [26], A quasi 3D formulation was validated and used to predict the appearance of modes due to the interaction of a rotor with spatially uniform steady and unsteady flow. These modes were first classified by [36] as “spinning modes”. In addition, further investigation was done on the results shown in [26]. The axial wavenumbers that were previously found to be purely convective were shown to be in part , “nearly convective” (shear) pressure modes. These were found to propagate in the axial direction with no loss in amplitude, thus never satisfying the cut-off condition.

## 2.2 Golubev and Atassi’s work

Similarly, a narrow annulus is once again studied but with a different theoretical and computational approach. The governing equations, similar to Wundrow [1] were still then linearized in terms of potential and rotation. As suggested by Case [7], a Fourier series analysis was used to conduct the normal mode analysis to find the corresponding wave numbers of the eigensystem. The findings show these fall into further classification which were previously denoted as purely convective and in part, nearly-convective wave modes. These two classifications of purely convective disturbance can be split into their “nearly-convected vorticity dominated” and “nearly-sonic pressure dominated” parts. These new results show the appearance of “nearly-sonic pressure dominated modes” which can propagate at varying phase speeds throughout the duct in both directions. The imposed Doppler shift from asymmetrical modes cause the sound propagate in the opposite direction of the mean flow swirl. A weak coupling relation relates the two and allows for the presence of vorticity - pressure mode coupling. Together, these nearly convected modes can be “identified with the purely convective gusts in a non swirling flow”. For the second group, these “nearly convected” vorticity dominated modes are further split as these disturbances approach the *critical layer*, i.e. the location at which the viscous effects

of the boundary layer begin to influence the coupling between modes. When both solid body and free vortex induced rotations are in the same direction, no instabilities arise from outside the critical layer. It was shown in later works that the influence of centrifugal and Coriolis forces created by the mean swirl prevent the decomposition of modes into their potential, rotational and entropic components. The paper ultimately proposes “ a generalized definition for incident rotational waves(gusts) is proposed which accounts for both the eigenmodes and the initial value solutions”

## 2.3 Review of the assessment of the numerical techniques

Kousen assessed the accuracy of the numerical discretization technique for a series of test cases using three sources [33] [37] and [6] ([10] [15] and [45] in Kousen’s work [25] respectively). The results were assessed by using various literature comparisons. The methodology was presented of uniform mean axial flows, but results for hard wall cases were presented by computing the order of accuracy for the first four radial modes (See Figures 4.1-4.4), . (Explain why this is MES and offer MMS as a source of verification and explain that MES is validation [31] [32] ). For a uniform axial flow, the axial wavenumbers can be computed from an analytical solution, where one of the key input parameters are the zero crossings of the derivative of the Bessel Function of the first kind . The values are presented [24] and are often referred to as separation constants for a circumferential and radial mode pair ; which are needed to compute the solution of the convective wave equation.

The axial wavenumber is found by using second-order differential convective wave equation for pressure using a fourth order accurate Runge-Kutta(RK) method [26] which was done to check against the results in [5] (Table 4.1 and 4.2 in [26]). The output parameter was  $\gamma/k$ . Each axial wave number can then be used to compute

the analytical radial mode using the exponential assumption. Axial wavenumbers from annular and cylindrical ducts with lined walls were compared to findings from Astley and Eversman [6] for uniform and sheared axial flow with liner (Table 4.3). The results taken were from a “high-order” RK scheme used. Axial wavenumbers from cylindrical ducts with hard walls were compared to findings from Shankar [33] in Table 4.4 of [26].

In recent years Maldonado et. al, [28] has made significant contributions in solution verification given the recent improvements in experimental measurement techniques. The work has presented test cases for lined ducts that have been compared to Kousen [26], Nijboer [29] and Peake [30] and show excellent comparison. The goal of this work is to contribute these efforts by conducting the method of manufactured solutions to offer clarity in using techniques often used in other verification and validation (V&V) studies.

### **2.3.1 The research questions, hypotheses, foreshadowed problems, or conjectures**

While these results confirm the findings of SWIRL and other LEE codes, this does not check if the equations that were programmed were entered correctly. While an emphasis on solution verification is vital, it should be coupled with code verification to determine the robustness and consistency of the algorithm. The method of manufactured solutions combined with order of accuracy verification is often used as a gold standard of code verification [31] and has been shown to provide an estimate of discretization error that can be computed before the final answer is obtained. Since the mid 2000’s, code verification literature has grown popular in the field of computational mathematics and physics due to its ability to conduct tests for numerical approximations of partial and ordinary differential equations. The MMS offers

a means of “manufacturing” an arbitrary solution by define functions for each term in the governing equation. Common practices and guidelines are offered in [32] to choose the fuunctions, but are phrased such that MMS can be widely applied. Since various numerical problems are unique in their treatment of spatial discretization, and boundary condtions , this work will describe the use of these guidelines and the nuances that have been taken to check the boundary conditon and radial derivatives used in SWIRL.

Knupp in Code Verification by the MMS [32] provides guidelines for creating manufactured soulutions which states,

1. The manufactured solutions should be composed of smooth analytic functions
2. The manufactured solutions should exercize every term in the governing equation that is being tested,
3. The solution should have non trivial derivatives.
4. The solution derivatives should be bounded by a small constant. In this case this constant should prevent the function from becoming greater than one.
5. The solution should not prevent the code from running
6. The solution should be defined on a connected subset of two- or three- dimensional space to allow flexibility in chosing the domain of the PDE.
7. The solution should coincide with the differential operators of the PDE. For example, the flux term in Fourier’s law of conduction requires  $T$  to be differentiable.

The goal is the to calculate an observed order of accuracy.

### 2.3.2 Calculation of Observed Order-of-Accuracy

To begin the method of manufactured solutions, the discretization error,  $\epsilon$  is defined as a function of radial grid spacing,  $\Delta r$

$$\epsilon = \epsilon(\Delta r)$$

The discretization error in the solution should be proportional to  $(\Delta r)^\alpha$  where  $\alpha > 0$  is the theoretical order for the computational method. The error for each grid is expressed as

$$\epsilon_{M_\theta}(\Delta r) = |M_{\theta,Analytic} - M_{\theta,calc}|$$

where  $M_{\theta,Analytic}$  is the tangential mach number that is defined from the speed of sound we also defined and the  $M_{\theta,calc}$  is the result from SWIRL. The  $\Delta r$  is to indicate that this is a discretization error for a specific grid spacing. Applying the same concept to the speed of sound,

If we define this error on various grid sizes and compute  $\epsilon$  for each grid, the observed order of accuracy can be estimated and compared to the theoretical order of accuracy. For instance, if the numerical solution is second-order accurate and the error is converging to a value, the L2 norm of the error will decrease by a factor of 4 for every halving of the grid cell size. Since the input variables should remain unchanged, the error for the axial and tangential mach number should be zero. As for the speed of sound, since we are using an analytic expression for the tangential mach number, we know what the theoretical result would be from the numerical integration technique as shown above. Similarly we define the discretization error for the speed of sound.

$$\epsilon_A(\Delta r) = |A_{Analytic} - A_{calc}|$$

For a perfect answer, we expect  $\epsilon$  to be zero. Since a Taylor series can be used to derive the numerical schemes, we know that the truncation of higher order terms is what indicates the error we expect from using a scheme that is constructed with such truncated Taylor series.

The expectation is that the error at each grid point  $j$  to satisfy the following,

$$0 = |A_{Analytic}(r_j) - A_{calc}(r_j)|$$

$$\tilde{A}_{Analytic}(r_j) = \tilde{A}_{calc}(r_j) + (\Delta r)^\alpha \beta(r_j) + H.O.T$$

where the value of  $\beta(r_j)$  does not change with grid spacing, and  $\alpha$  is the asymptotic order of accuracy of the method. It is important to note that the numerical method recovers the original equations as the grid spacing approached zero.

Subtracting  $A_{Analytic}$  from both sides gives

$$A_{calc}(r_j) - A_{Analytic}(r_j) = A_{Analytic}(r_j) - A_{Analytic}(r_j) + \beta(r_j)(\Delta r)^\alpha$$

$$\epsilon_A(r_j)(\Delta r) = \beta(r_j)(\Delta r)^\alpha$$

To estimate the order of accuracy of the accuracy, the global errors are calculated by taking the L2 Norm of the error which is denoted as  $\hat{\epsilon}_A$

$$\hat{\epsilon}_A = \sqrt{\frac{1}{N} \sum_{j=1}^N \epsilon(r_j)^2}$$

$$\hat{\beta}_A(r_j) = \sqrt{\frac{1}{N} \sum_{j=1}^N \beta(r_j)^2}$$

As the grid density increases,  $\hat{\beta}$  should asymptote to a constant value. Given two grid densities,  $\Delta r$  and  $\sigma\Delta r$ , and assuming that the leading error term is much larger than any other error term,

$$\begin{aligned}\hat{\epsilon}_{grid1} &= \hat{\epsilon}(\Delta r) = \hat{\beta}(\Delta r)^\alpha \\ \hat{\epsilon}_{grid2} &= \hat{\epsilon}(\sigma\Delta r) = \hat{\beta}(\sigma\Delta r)^\alpha \\ &= \hat{\beta}(\Delta r)^\alpha \sigma^\alpha\end{aligned}$$

The ratio of two errors is given by,

$$\begin{aligned}\frac{\hat{\epsilon}_{grid2}}{\hat{\epsilon}_{grid1}} &= \frac{\hat{\beta}(\Delta r)^\alpha}{\hat{\beta}(\Delta r)^\alpha} \sigma^\alpha \\ &= \sigma^\alpha\end{aligned}$$

Thus,  $\alpha$ , the asymptotic rate of convergence is computed as follows

$$\alpha = \frac{\ln \frac{\hat{\epsilon}_{grid2}}{\hat{\epsilon}_{grid1}}}{\ln(\sigma)}$$

For example ,a doubling of grid points has  $\sigma = 1/2$ ,

$$\alpha = \frac{\ln(\hat{\epsilon}(\frac{1}{2}\Delta r)) - \ln(\hat{\epsilon}(\Delta r))}{\ln(\frac{1}{2})}$$

## 2.4 Conclusion

This review discusses the development of the unsteady linearized equations, and how improvements in the modal analysis capture more families of mechanisms of noise generation within non-uniform swirling flow turbomachinery flow. While the literature presented offers a measure of verification and validation through the use of the Method of Exact Solutions, the Method of Manufactured Solutions offers a level of code verification which allows for error checking by computing the approximate order of accuracy for a given numerical scheme, which is independent of the final answer, which in this case is the axial wavenumber. The next chapter will outline the methodology and techniques used when applying MMS to SWIRL. The methods consist of unique treatment of boundary conditions using fairing functions as well as an example of using a summation to generate arbitrary functions as manufactured solutions which has the dual benefit of giving a large number of derivatives but allows for high gradients in specific locations along the domain of the MS. The use of open-source widely available functions in Python were used to symbolically create the MS and then used to generate FORTRAN code that will compute the MS for code comparison.



# Chapter 3

## Theoretical Framework and Methods

### 3.1 Introduction

This chapter will outline the steady and unsteady aerodynamic models used for this study. The MMS procedure as it is used in this study will be described. The summation method used to generate symbolic expression will be briefly described. This chapter will also present the use of fairing functions to impose the equivalent boundary conditions used in the numerical approximation. The procedure for calculating the approximated rate of convergence for a system of equations is also presented.

### 3.2 Governing Equations for Compressible, Inviscid Flow

The governing equations for an isentropic, inviscid, compressible gas with density,  $\rho$ , velocity,  $\vec{V}$ , and pressure,  $p$  describe the conservation of mass, momentum, and energy for a given domain in Equations (3.1, 3.2, 3.2) respectively.

$$\frac{D\rho}{Dt} = -\rho \nabla \cdot \vec{V} \quad (3.1)$$

$$\frac{D\vec{V}}{Dt} = -\frac{\nabla p}{\rho} + \vec{g} \quad (3.2)$$

$$\frac{Ds}{Dt} = 0 \quad (3.3)$$

where  $D/Dt$  is the material derivative operator,,

$$\frac{D}{Dt} = \frac{\partial}{\partial t} + \nabla \cdot \vec{V} \quad (3.4)$$

For this model, the domain is assumed to be uniformly cylindrical. Therefore the flow is assumed to be asymmetric, then the radial velocity component is zero. With this considered, the velocity vector , $\vec{V}$  in cylindrical coordinates become,

$$\vec{V}(r, \theta, x) = v_x(r)\hat{e}_x + v_\theta(r)\hat{e}_\theta \quad (3.5)$$

where  $\hat{e}_x$  and  $\hat{e}_\theta$  are unit vectors for the axial and tangential directions. The gradient operator , $\nabla$  in cylindrical coordinates, is

$$\vec{\nabla} = \hat{e}_r \frac{\partial}{\partial r} + \frac{1}{r} \hat{e}_\theta \frac{\partial}{\partial \theta} + \frac{\partial}{\partial z} \hat{e}_z = 0 \quad (3.6)$$

To close the problem and to write in terms of pressure, the thermodynamic relation for the speed of sound is used

$$A^2 = \left. \frac{\partial p}{\partial \rho} \right|_s \quad (3.7)$$

Utilizing the equation of state in differential form and with material derivatives

$$\frac{Dp}{Dt} = A^2 \frac{D\rho}{Dt} + \frac{\partial p}{\partial s} \bigg|_{\rho} \frac{Ds}{Dt} \quad (3.8)$$

The conervation of energy can be rewritten in terms of pressure, by using 3.7 and 3.8

$$\frac{Dp}{Dt} = A^2 \frac{D\rho}{Dt}. \quad (3.9)$$

Using the 3.1 in non-conservative form and the definition  $A^2 = \gamma p / \rho$  (See Appendix for derivation)

$$\frac{Dp}{Dt} + \gamma p (\nabla \cdot \vec{V}) = 0. \quad (3.10)$$

Expanding equations ( 3.1, 3.2, 3.10 ) with the corresponding cylindrical expressions become,

$$\frac{\partial \rho}{\partial t} + v_r \frac{\partial \rho}{\partial r} + \frac{v_\theta}{r} \frac{\partial \rho}{\partial \theta} + v_x \frac{\partial \rho}{\partial x} + \rho \left( \frac{1}{r} \frac{\partial(rv_r)}{\partial r} + \frac{1}{r} \frac{\partial v_\theta}{\partial \theta} + \frac{\partial v_x}{\partial x} \right) = 0 \quad (3.11)$$

$$\frac{\partial v_r}{\partial t} + v_r \frac{\partial v_r}{\partial r} + \frac{v_\theta}{r} \frac{\partial v_r}{\partial \theta} - \frac{v_\theta^2}{r} + v_x \frac{\partial v_r}{\partial x} = -\frac{1}{\rho} \frac{\partial p}{\partial r} \quad (3.12)$$

$$\frac{\partial v_\theta}{\partial t} + v_r \frac{\partial v_\theta}{\partial r} + \frac{v_\theta}{r} \frac{\partial v_\theta}{\partial \theta} + \frac{v_r v_\theta}{r} + v_x \frac{\partial v_\theta}{\partial x} = -\frac{1}{\rho r} \frac{\partial p}{\partial \theta} \quad (3.13)$$

$$\frac{\partial v_x}{\partial t} + v_r \frac{\partial v_x}{\partial r} + \frac{v_\theta}{r} \frac{\partial v_x}{\partial \theta} + v_x \frac{\partial v_x}{\partial x} = -\frac{1}{\rho} \frac{\partial p}{\partial x} \quad (3.14)$$

$$\frac{\partial p}{\partial t} + v_r \frac{\partial p}{\partial r} + \frac{v_\theta}{r} \frac{\partial p}{\partial \theta} + v_x \frac{\partial p}{\partial x} + \gamma p \left( \frac{1}{r} \frac{\partial(rv_r)}{\partial r} + \frac{1}{r} \frac{\partial v_\theta}{\partial \theta} + \frac{\partial v_x}{\partial x} \right) = 0 \quad (3.15)$$

### 3.3 Nonuniformities from swirling mean flow

If the mean flow contains a swirling component, i.e. a velocity vector in the tangential direction, the mean quantities, pressure , density are non-uniform, thus also changing the speed of sound. By integrating the radial momentum equation, an expression for the speed of sound was established to account for the resulting

nonuniformities due to rotations in the flow.

$$p = \int_{r_{min}}^{r_{max}} \frac{\rho v_{\theta}^2}{r} dr \quad (3.16)$$

where  $r_{min}$  and  $r_{max}$  are the bounds of the radius. Since the flow is isentropic, the pressure is related to the speed of sound through  $\nabla p = A^2 \nabla \rho$ ; which is used to compute  $\rho$ . With the relationship  $A^2 = \gamma p / \rho$ , the speed of sound is found to be,

$$\tilde{A}(\tilde{r}) = \exp \left[ \left( \frac{1-\gamma}{2} \right) \int_{\tilde{r}}^1 \frac{M_{\theta}}{\tilde{r}} \partial \tilde{r} \right] \quad (3.17)$$

The appendix shows how the speed of sound was extracted. For special cases of swirling flow, the relation to between the speed of sound and the tangential velocity can be found. Expressions can be derived for free vortex , and/or solid body swirl. The non-dimesionalization is shown in the next section.

### 3.4 Linearizing the Governing Equations

To linearize the Euler equations, we substitute each flow variable with its equivalent mean and perturbation components. Note that the mean term is only a function of space whereas the perturbation component is a dependent on both space and time (functional dependence is not explicitly written with each variable). Assuming that we can divide the variable into a known laminar flow solution to the governing equations and a small amplitude perturbation solution,

$$v_r = V_r(x) + v'_r \quad (3.18)$$

$$v_\theta = V_\theta + v'_\theta \quad (3.19)$$

$$v_x = V_x + v'_x \quad (3.20)$$

$$p = \bar{p} + p' \quad (3.21)$$

$$\rho = \bar{\rho} + \rho' \quad (3.22)$$

One key assumption is that the perturbation quantites,  $\tilde{p}$ ,  $\tilde{v}_r, \tilde{v}_\theta$ , and  $\tilde{v}_x$  , are all exponential and that they are solely a function of radius,

$$v'_r = v_r(r)e^{i(k_x x + m\theta - \omega t)} \quad (3.23)$$

$$v'_\theta = v_\theta(r)e^{i(k_x x + m\theta - \omega t)} \quad (3.24)$$

$$v'_x = v_x(r)e^{i(k_x x + m\theta - \omega t)} \quad (3.25)$$

$$p' = p(r)e^{i(k_x x + m\theta - \omega t)} \quad (3.26)$$

There are a few important assumptions that will be utilized,

- The small disturbances are infinitesimal (thus linearized)
- Neglect second order terms.
- The continuity equation is comprised of mean velocity components. This is subtracted off in each of the governing equations

The following relationships were utilized to simplify the linearized equations,

$$\frac{\partial P}{\partial r} = \frac{\bar{\rho} V_\theta^2}{r}$$

$$\gamma P = \bar{\rho} A^2$$

$$\rho' = \frac{1}{A^2} p'$$

Note that the momentum equation in the  $\theta$  and  $x$  directions remain unchanged.

The term  $\frac{\partial(rv'_r)}{\partial r} = \frac{\partial(r)}{\partial r}v'_r + \frac{\partial v'_r}{\partial r}r$  in the Energy equation

$$\begin{aligned} \frac{1}{\bar{\rho} A^2} \left( \frac{\partial p'}{\partial t} + \frac{V_\theta}{r} \frac{\partial p'}{\partial \theta} + V_x \frac{\partial p'}{\partial x} \right) + \frac{V_\theta^2}{A^2 r} v'_r + \frac{\partial v'_r}{\partial r} + \frac{v'_r}{r} + \frac{1}{r} \frac{\partial v'_\theta}{\partial \theta} + \frac{\partial v'_x}{\partial x} &= 0 \\ \frac{\partial v'_r}{\partial t} + \frac{V_\theta}{r} \frac{\partial v'_r}{\partial \theta} - \frac{2V_\theta v'_\theta}{r} + V_x \frac{\partial v'_r}{\partial x} &= \frac{1}{\bar{\rho}} \frac{\partial p'}{\partial r} + \frac{V_\theta}{\bar{\rho} r A^2} p' \\ \frac{\partial v'_\theta}{\partial t} + v'_r \frac{\partial V_\theta}{\partial r} + \frac{V_\theta}{r} \frac{\partial v'_\theta}{\partial \theta} + \frac{v'_r V_\theta}{r} + V_x \frac{\partial v'_\theta}{\partial x} &= -\frac{1}{\bar{\rho} r} \frac{\partial p'}{\partial \theta} \\ \frac{\partial v'_x}{\partial t} + v'_r \frac{\partial V_x}{\partial r} + \frac{V_\theta}{r} \frac{\partial v'_x}{\partial \theta} + V_x \frac{\partial v'_x}{\partial x} &= -\frac{1}{\bar{\rho}} \frac{\partial p'}{\partial x} \end{aligned}$$

Substituting Equation (3.26) into the linearized equations will give us the final governing equations.

$$\begin{aligned} i \left( -\omega + \frac{m}{r} + k_x V_x \right) v_r - \frac{2\bar{v}_\theta}{r} v_\theta &= -\frac{1}{\bar{\rho}} \frac{\partial P}{\partial r} + \frac{V_\theta^2}{A^2} \frac{1}{\bar{\rho} r} p \\ i \left( -\omega + \frac{m}{r} + k_x V_x \right) v_\theta + \left( \frac{V_\theta}{r} + \frac{\partial V_\theta}{\partial r} \right) v_\theta &= -\frac{m}{\bar{\rho} r} p \\ i \left( -\omega + \frac{m V_\theta}{r} + k_x V_x \right) v_x + \frac{\partial V_x}{\partial r} v_r &= -\frac{i k_x}{\bar{\rho}} p \\ \frac{1}{\bar{\rho} A^2} \left( -i\omega + \frac{i m V_\theta}{r} + i k_x V_x \right) p(r) + \frac{V_\theta^2}{A^2 r} v_r + \frac{v_r}{r} + \frac{\partial v_r(r)}{\partial r} + \frac{i m}{r} v_\theta(r) + i k_x v_x(r) &= 0 \end{aligned}$$

### 3.5 Non-Dimensionalization

Defining

$$r_T = r_{max}$$

$$A_T = A(r_{max})$$

$$k = \frac{\omega r_T}{A_T}$$

$$\bar{\gamma} = k_x r_T$$

$$\tilde{r} = \frac{r}{r_T}$$

$$\frac{\partial}{\partial r} = \frac{\partial \tilde{r}}{\partial r} \frac{\partial}{\partial \tilde{r}} = \frac{1}{r_T} \frac{\partial}{\partial \tilde{r}}$$

$$V_\theta = M_\theta A$$

$$V_x = M_x A$$

$$\tilde{A} = \frac{A}{A_T}$$

$$v_x = \tilde{v}_x A$$

$$v_r = \tilde{v}_r A$$

$$v_\theta = \tilde{v}_\theta A$$

$$p = \tilde{p} \bar{\rho} A^2$$

Substituting in yields ,

$$i \left[ -\frac{k}{\tilde{A}} + \frac{m M_\theta}{\tilde{r}} + \bar{\gamma} M_x \right] \tilde{v}_r - \frac{2 M_\theta \tilde{v}_\theta}{\tilde{r}} = -\frac{\partial \tilde{p}}{\partial \tilde{r}} - (\gamma - 1) \frac{\gamma M_\theta}{\tilde{r}} \tilde{p} \quad (3.27)$$

$$i \left[ -\frac{k}{\tilde{A}} + \frac{m M_\theta}{\tilde{r}} + \bar{\gamma} M_x \right] \tilde{v}_\theta + \left( \frac{M_\theta}{\tilde{r}} + \frac{1}{A} \frac{\partial M_\theta A}{\partial \tilde{r}} \right) \tilde{v}_r = \frac{i m}{\tilde{r}} \tilde{p} \quad (3.28)$$

$$i \left[ -\frac{k}{\tilde{A}} + \frac{m M_\theta}{\tilde{r}} + \bar{\gamma} M_x \right] \tilde{v}_x + \frac{1}{A} \frac{\partial M_x A}{\partial \tilde{r}} \tilde{v}_r = -i \bar{\gamma} \tilde{p} \quad (3.29)$$

$$i \left[ -\frac{k}{\tilde{A}} + \frac{m M_\theta}{\tilde{r}} + \bar{\gamma} M_x \right] \tilde{p} + \frac{M_\theta^2}{\tilde{r}} \tilde{v}_r + \frac{\partial \tilde{v}_r}{\partial \tilde{r}} + \frac{1}{A} \frac{\partial A}{\partial \tilde{r}} v_r + \frac{\tilde{v}_r}{\tilde{r}} + \frac{i m}{\tilde{r}} \tilde{v}_\theta + i \bar{\gamma} \tilde{v}_x = 0 \quad (3.30)$$

The mean flow derivatives  $\partial A / \partial r$  and  $\partial(\bar{\rho} A^2) / \partial r$

$$i \left[ -\frac{k}{\tilde{A}} + \frac{mM_\theta}{\tilde{r}} + \bar{\gamma}M_x \right] \tilde{v}_r - \frac{2M_\theta \tilde{v}_\theta}{\tilde{r}} = -\frac{\partial \tilde{p}}{\partial \tilde{r}} - (\gamma - 1) \frac{\gamma M_\theta}{\tilde{r}} \tilde{p} \quad (3.31)$$

$$i \left[ -\frac{k}{\tilde{A}} + \frac{mM_\theta}{\tilde{r}} + \bar{\gamma}M_x \right] \tilde{v}_\theta + \left( \frac{M_\theta}{\tilde{r}} + \frac{1}{A} \frac{\partial M_\theta A}{\partial \tilde{r}} \right) \tilde{v}_r = \frac{im}{\tilde{r}} \tilde{p} \quad (3.32)$$

$$i \left[ -\frac{k}{\tilde{A}} + \frac{mM_\theta}{\tilde{r}} + \bar{\gamma}M_x \right] \tilde{v}_x + \frac{1}{A} \frac{\partial M_x A}{\partial \tilde{r}} \tilde{v}_r = -i\bar{\gamma} \tilde{p} \quad (3.33)$$

$$i \left[ -\frac{k}{\tilde{A}} + \frac{mM_\theta}{\tilde{r}} + \bar{\gamma}M_x \right] \tilde{p} + \frac{M_\theta^2}{\tilde{r}} \tilde{v}_r + \frac{\partial \tilde{v}_r}{\partial \tilde{r}} + \frac{1}{A} \frac{\partial A}{\partial \tilde{r}} \tilde{v}_r + \frac{\tilde{v}_r}{\tilde{r}} + \frac{im}{\tilde{r}} \tilde{v}_\theta + i\bar{\gamma} \tilde{v}_x = 0 \quad (3.34)$$

Defining,  $\lambda = -i\bar{\gamma}$

and defining

$$\{\bar{x}\} = \begin{Bmatrix} \tilde{v}_r \\ \tilde{v}_\theta \\ \tilde{v}_x \\ \tilde{p} \end{Bmatrix}$$

The governing equations can be written in the form of  $[A]x - \lambda[B]x$

$$\begin{bmatrix} -i \left( \frac{k}{A} - \frac{mM_\theta}{\tilde{r}} \right) - \lambda M_x & -\frac{2M_\theta}{\tilde{r}} & 0 & \frac{\partial}{\partial \tilde{r}} + \frac{\gamma-1}{\tilde{r}} \\ \frac{M_\theta}{\tilde{r}} + \frac{\partial M_\theta}{\partial \tilde{r}} + \left( \frac{\gamma-1}{2} \right) \frac{M_\theta^2}{\tilde{r}} & -i \left( \frac{k}{A} - \frac{mM_\theta}{\tilde{r}} \right) - \lambda M_x & 0 & \frac{im}{\tilde{r}} \\ \frac{\partial M_x}{\partial \tilde{r}} + \left( \frac{\gamma-1}{2} \right) \frac{M_x M_\theta^2}{\tilde{r}} & 0 & -i \left( \frac{k}{A} - \frac{mM_\theta}{\tilde{r}} \right) - \lambda M_x & -\lambda \\ \frac{\partial}{\partial \tilde{r}} + \frac{\gamma+1}{2} \frac{M_\theta^2}{\tilde{r}} + \frac{1}{\tilde{r}} & \frac{im}{\tilde{r}} & -\lambda & -i \left( \frac{k}{A} - \frac{mM_\theta}{\tilde{r}} \right) - \lambda M_x \end{bmatrix} \bar{x} = 0$$



(place holder for analytics)

# Chapter 4

## Verification and Validation Techniques for Numerical Approximations

### 4.1 Introduction

The Method of Manufactured Solutions (MMS) is a process for generating an analytical solution for a code that provides the numerical solution for a given domain. The goal of MMS is to establish a manufactured solution that can be used to establish the accuracy of the code within question. For this study, SWIRL, a code used to calculate the radial modes within an infinitely long duct is being validated through code verification. SWIRL accepts a given mean flow and uses numerical integration to obtain the speed of sound. The integration technique is found to be the composite trapezoidal rule through asymptotic error analysis.

For SWIRL, the absolute bare minimum requirement is to define the corresponding flow components for the domain of interest. SWIRL assumes no flow in the radial direction, leaving only two other components, axial and tangential for a 3D cylindrical domain. Since SWIRL is also non dimensionalized, the mean flow components are

defined using the Mach number. SWIRL uses the tangential mach number to obtain the speed of sound using numerical integration. The speed of sound is then used to find the rest of the primitive variables for the given flow.

### 4.1.1 Examining Convergence Using Multiple Grids

When repeating the simulation while increasing the number of grid points is standard practice when conducting a numerical approximation. The discretization errors that initially arise should asymptotically approach zero, excluding computer round-off error.

Although it is desirable to know the error band for the results obtained from a fine grid, the study may require a coarse grid due to time constraints for design iteration. Furthermore, as the grid gets finer, the computational time required increases. So it is desirable to compute the discretization on grids with fewer points to get a sense of where the asymptotic range is located. The approach for generating the series of grids is to generate a grid with what the user would consider small or fine grid spacing, reaching the upper limit of one's tolerance for generating a grid. Otherwise, the finest grid that requires the least amount of computation on that grid to converge should be chosen. Then coarser grids can be obtained by removing every other grid point. Finally, the number of iterations can be increased to create additional levels of coarse grids. For example, in generating the fine grid, one can choose the number of coarser grids by satisfying the following relation,

$$N = (2^n)m + 1 \tag{4.1}$$

where,  $N$  is the number of grid points,  $n$  is the iteration level, and  $m$  is an arbitrary integer. The base 2 has the effect of doubling grid points. However  $m$  can change between iterations which will allow for grids which are fractions of double.

One can use the finest grid that was run to determine how to iterate from a coarser grid up to a finer one. Note that the number of grid points does not to be doubled each time, however the grid refinement should be such that the ratio between grid spacing it is less than 0.91 since it is easier to determine which errors occur from

discretization as opposed to computer round-off error or iterative convergence errors.

For this work, the number of grid points will be computed using the following

#### 4.1.2 Calculation of Observed Order-of-Accuracy

The numerical scheme used to perform the integration of the tangential velocity will have a theoretical order-of-accuracy. To find the theoretical order-of-accuracy, the discretization error must first be defined. The error,  $\epsilon$ , is a function of grid spacing,  $\Delta r$

$$\epsilon = \epsilon(\Delta r)$$

The discretization error in the solution should be proportional to  $(\Delta r)^\alpha$  where  $\alpha > 0$  is the theoretical order for the computational method. An error between two quantities can expressed as

$$\epsilon(\Delta r) = |f_{analytic} - f_{calc}|$$

where  $f_{analytic}$  is the function value of an analytic solution and  $f_{calc}$  represents some calculated value. The  $\Delta r$  is to indicate that this is a discretization error for a specific grid spacing.

If we define this error on various grid sizes and compute  $\epsilon$  for each grid, the observed order of accuracy can be estimated and compared to the theoretical order of accuracy. For instance, if the numerical solution is second-order accurate and the error is converging to a value, the  $L_2$  norm of the error will decrease by a factor of 4 for every halving of the grid cell size.

For a perfect answer, we expect  $\epsilon$  to be zero. Since a Taylor series can be used to derive the numerical schemes, we know that the truncation of higher order terms is what indicates the error we expect from using a scheme that is constructed with

such truncated Taylor series.

The error at each grid point  $j$  is expected to satisfy the following,

$$0 = |f_{analytic}(r_j) - f_{calc}(r_j)|$$

$$f_{analytic}(r_j) = f_{calc}(r_j) + (\Delta r)^\alpha \beta(r_j) + H.O.T$$

where the value of  $\beta(r_j)$  does not change with grid spacing, and  $\alpha$  is the asymptotic order of accuracy of the method. It is important to note that the numerical method recovers the original equations as the grid spacing approached zero. It is important to note that  $\beta$  represents the first derivative of the Taylor Series. Subtracting  $f_{analytic}$  from both sides gives,

$$f_{calc}(r_j) - f_{analytic}(r_j) = f_{analytic}(r_j) - f_{analytic}(r_j) + \beta(r_j)(\Delta r)^\alpha$$

$$\epsilon(r_j)(\Delta r) = \beta(r_j)(\Delta r)^\alpha$$

To estimate the order of accuracy of the accuracy, we define the global errors by calculating the L2 Norm of the error which is denoted as  $\hat{\epsilon}$

$$\hat{\epsilon} = \sqrt{\frac{1}{N} \sum_{j=1}^N \epsilon(r_j)^2}$$

$$\hat{\beta}(r_j) = \sqrt{\frac{1}{N} \sum_{j=1}^N \beta(r_j)^2}$$

As the grid density increases,  $\hat{\beta}$  should asymptote to a constant value. Given two

grid densities,  $\Delta r$  and  $\sigma\Delta r$ , and assuming that the leading error term is much larger than any other error term,

$$\begin{aligned}\hat{\epsilon}_{grid1} &= \hat{\epsilon}(\Delta r) = \hat{\beta}(\Delta r)^\alpha \\ \hat{\epsilon}_{grid2} &= \hat{\epsilon}(\sigma\Delta r) = \hat{\beta}(\sigma\Delta r)^\alpha \\ &= \hat{\beta}(\Delta r)^\alpha \sigma^\alpha\end{aligned}$$

The ratio of two errors is given by,

$$\begin{aligned}\frac{\hat{\epsilon}_{grid2}}{\hat{\epsilon}_{grid1}} &= \frac{\hat{\beta}(\Delta r)^\alpha}{\hat{\beta}(\Delta r)^\alpha} \sigma^\alpha \\ &= \sigma^\alpha\end{aligned}$$

Thus,  $\alpha$ , the asymptotic rate of convergence is computed as follows

$$\alpha = \frac{\ln \frac{\hat{\epsilon}_{grid2}}{\hat{\epsilon}_{grid1}}}{\ln(\sigma)}$$

Defining for a doubling of grid points ,

$$\alpha = \frac{\ln(\hat{\epsilon}(\frac{1}{2}\Delta r)) - \ln(\hat{\epsilon}(\Delta r))}{\ln(\frac{1}{2})}$$

## 4.2 Methods

The SWIRL code requires two mean flow parameters as a function of radius,  $M_x$ , and  $M_\theta$ . Afterwards, the speed of sound,  $\tilde{A}$  is calculated by integrating  $M_\theta$  with respect to  $r$ . To verify that SWIRL is handling and returning the accompanying mean flow parameters, the error between the mean flow input and output variables are computed. Since the trapezoidal rule is used to numerically integrate  $M_\theta$ , the discretization error and order of accuracy is computed. Since finite differencing schemes are to be used on the result of this integration, it is crucial to accompany the integration with methods of equal or less order of accuracy. This will be determined by applying another MMS on the eigenproblem which will also have an order of accuracy.



### 4.2.1 Procedure

There are a few constraints and conditions that must be followed in order for the analytical function to work with SWIRL,

- The mean flow and speed of sound must be real and positive. This will occur if a speed of sound is chosen such that the tangential mach number is imaginary
- The derivative of the speed of sound must be positive
- Any bounding constants used with the mean flow should not allow the total Mach number to exceed one.
- the speed of sound should be one at the outer radius of the cylinder

Given these constraints,  $\tanh(r)$  is chosen as a function since it can be modified to meet the conditions above. Literature (The tanh method: A tool for solving certain classes of nonlinear evolution and wave equations) is a paper that demonstrates the strength of using tanh functions. One additional benefit of  $\tanh(r)$  is that it is bounded between one and negative one, i.e.

- As  $r \rightarrow \infty$   $\tanh(r) \rightarrow 1$
- As  $-r \rightarrow -\infty$   $\tanh(r) \rightarrow -1$

To test the numerical integration method,  $M_\theta$  is defined as a result of differentiating the speed of sound,  $A$ . This is done opposed to integrating  $M_\theta$  analytically. However, an analytical function can be defined for  $M_\theta$ , which can then be integrated to find what  $\tilde{A}$  should be. Instead, the procedure of choice is to back calculate what the appropriate  $M_\theta$  is for a given expression for  $\tilde{A}$ . Since it is easier to take derivatives, we will solve for  $M_\theta$  using Equation ?? ,

### 4.2.2 Tanh Summation Formulation

Knupp’s Code Verification by the Method of Manufactured Solution (MMS) provides “guidelines” for creating a manufactured solution (MS) such that the observed order of accuracy will approach a theoretical order of accuracy as the number of grid points are reduced from one iteration to the next. While these guidelines offer a road map, there are choices that are left to the investigator that would benefit from additional examples. The first guideline gives the user a free choice of the MS as long as it is smooth. The benefit of the tanh summation method (TSM) reduces the difficulty in defining a sufficient MS by providing a general summation formulation that allows the user to Vary the number of terms in the MS, and the MS behavior without manually changing terms in the MS symbolic expression.

The general form of the MS will be a summation of *tanh* bounded between zero and one. A MS created with the TSM can provide a significant result for a numerical differencing/integration technique by having inflection points of each *tanh* at various locations along the domain, giving a stair like slope. While the TSM can add a layer of complexity to the MS that may not be needed, writing the formulation in a summation lends itself to iterative loops that can be coded, thus reducing the need for manual adjust of the MS, which can be an initial hurdle when performing MMS.

## 4.3 General form of a Hyperbolic Tangent

$$R = A \tanh(B(x - C)) \tag{4.2}$$

$$L = A \tanh(B(C - E)) \tag{4.3}$$

$$y = R + L + D \tag{4.4}$$

where

- $R \equiv$  The value of the hyperbolic tangent. The variable  $R$  represents a “right” facing hyperbolic tangent kink.
- $A \equiv$  magnitude factor that increases or decreases the asymptotic limits  $\lim_{x \rightarrow -\infty} = -1$   $\lim_{x \rightarrow \infty} = 1$
- $B \equiv$  “steepness” of the hyperbolic tangent
- $C \equiv$  The shift in inflection point of the hyperbolic tangent along the  $x$  axis
- $D \equiv$  The shift in inflection point of the hyperbolic tangent along the  $y$  axis
- $E \equiv x_{i=imax}$
- $x$  The domain.  $x_i$  is used to indicate grid point indices.

The idea is to sum up an arbitrary amount of tangents that will be bounded by zero and one.

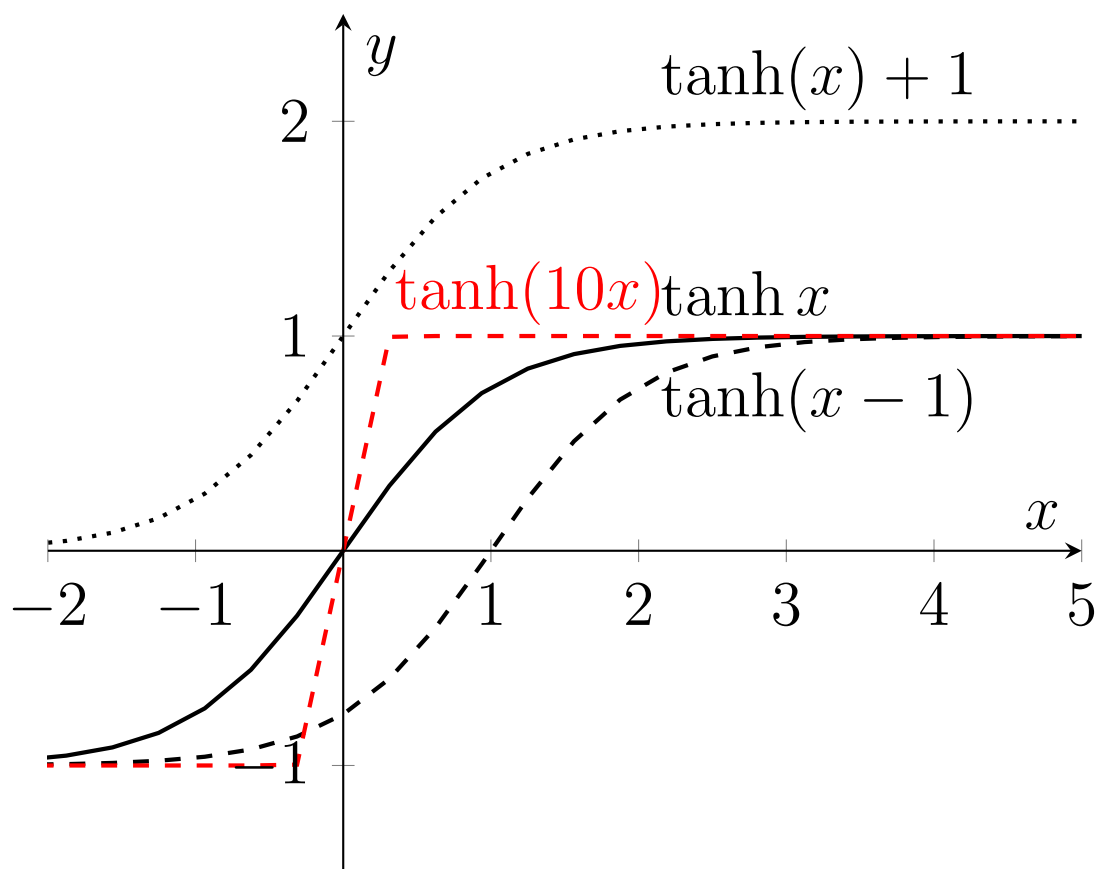
Now the goal is to generalize this formulation such that we can add up terms.  $A$  is determined by setting a maximum amplitude for each  $\tanh$  function by  $A = A_{max}/n$ . Note that amplitude can be different for each term but is chosen to be the same. A parameter  $\hat{x} = (x - x_{min})/(x_{max} - x_{min})$  scales the domain to be between the minimum and maximum bounds.

$$R_{ij} = A \tanh(B(x_i - C_j)) \quad (4.5)$$

$$L_j = A \tanh(B(C_j - E)) \quad (4.6)$$

$$y = \sum_{j=1}^n R_{ij} + \sum_{j=1}^n L_j + D \quad (4.7)$$

The function `TanhMethod` does this procedure.



Setting  $A = 1/16$  and  $C_1 = 0$  ,  $C_2 = 0.75$  ,  $C_3 = 1$  ,  $D = 1$ ,  $E = 1$  and  $B = 10$

$$\sum_{j=1}^3 R_{ij} = 1/16 \tanh(10(\hat{x}_i)) + 1/16 \tanh(10(\hat{x}_i - 0.75)) + 1/16 \tanh(10(\hat{x}_i - 1)) \quad (4.8)$$

$$\sum_{j=1}^3 L_j = 1/16 \tanh(10(-1)) + 1/16 \tanh(10(0.75 - 1)) + 1/16 \tanh(10(1 - 1)) \quad (4.9)$$

The simplified expression becomes,

$$y = \frac{1}{16} \tanh\left(\frac{100}{9}r - \frac{100}{9}\right) + \frac{1}{16} \tanh\left(\frac{100}{9}r - \frac{55}{9}\right) + \frac{1}{16} \tanh\left(\frac{100}{9}r - \frac{10}{9}\right) + \frac{7}{8} \quad (4.10)$$

A tanh summation method was constructed to make a manufactured solution with strong changes in slope. This ensures that the numerical approximation will not give trivial answers. then for some functions we need to impose boundary conditions. We will demonstrate how the careless implementation of a boundary condition can lead to close approximations on the interior. The speed of sound is defined with the subscript *analytic* to indicate that this is the analytical function of choice and has no physical relevance to the actual problem.

$$\tilde{A}_{analytic} = \Lambda + k_1 \tanh(k_2(\tilde{r} - \tilde{r}_{max})),$$

where,

$$\Lambda = 1 - k_1 \tanh(k_2(1 - \tilde{r}_{max})),$$

When,  $\tilde{r} = \tilde{r}_{max}$  ,  $\tilde{A}_{analytic} = 1$ . Taking the derivative with respect to  $\tilde{r}$ ,

$$\begin{aligned}\frac{\partial \tilde{A}_{analytic}}{\partial \tilde{r}} &= (1 - \tanh^2((r - r_{max})k_2))k_1k_2, \\ &= \frac{k_1k_2}{\cosh^2((r - r_{max})k_2)}.\end{aligned}$$

Substitute this into the expression for  $M_\theta$  in Equation ??,

$$M_\theta = \sqrt{2} \sqrt{\frac{rk_1k_2}{(\kappa - 1)(\tanh((r - r_{max})k_2)k_1 + \tanh((r_{max} - 1)k_2)k_1 + 1)\cosh^2((r - r_{max})k_2)}}$$

Now that the mean flow is defined, the integration method used to obtain the speed of sound

Initially the source terms were defined without mention of the indices of the matrices they make up. In other words, there was no fore sight on the fact that these source terms are sums of the elements within A,B, and X. To investigate the source terms in greater detail, the FORTRAN code that calls the source terms will output the terms within the source term and then sum them, instead

of just their sum. i  $[A]x = \lambda[B]x$

which can be rearranged as,

$$[A]x - \lambda[B]x = 0$$

Here,  $x$  is an eigenvector composed of the perturbation variables,  $v_r, v_\theta, v_x, p$  and  $\lambda$  is the associated eigenvalue, (Note:  $\lambda = -i\bar{\gamma}$ )

Writing this out we obtain  $\dots$ .

Linear System of Equations:

$$-i \left( \frac{k}{A} - \frac{m}{r} M_\theta \right) v_r - \frac{2}{r} M_\theta v_\theta + \frac{dp}{dr} + \frac{(\kappa - 1)}{r} M_\theta^2 p - \lambda M_x v_r = S_1 \quad (4.11)$$

Using matrix notation,

$$A_{11}x_1 - A_{12}x_2 + A_{14}x_4 - \lambda B_{11}x_1 = S_1 \quad (4.12)$$

But  $A_{14}$  and  $A_{41}$  in Kousen's paper only has the derivative operator. Since I am currntly writing the matrix out term by term and not doing the matrix math to obtain the symbolic expressions, I will define  $A_{14}$  with  $dp/dr$  and  $A_{41}$  with  $dv_r/dr$ . Similarly,

$$A_{21}x_1 - A_{22}x_2 + A_{24}x_4 - \lambda B_{22}x_2 = S_2 \quad (4.13)$$

$$A_{31}x_1 - A_{33}x_3 - \lambda(B_{33}x_3 + B_{34}x_4) = S_3 \quad (4.14)$$

$$A_{41}x_1 + A_{42}x_2 + A_{44}x_4 - \lambda(B_{33}x_3 + B_{44}x_4) = S_4 \quad (4.15)$$

Now we can begin looking at the source terms, term by term. They each should also converge at a known rate

Goal: How can we modify a manufactured solution such that the endpoints are suitable for comparison against a codes boundary condition implementation

## 4.4 Setting Boundary Condition Values Using a Fairing Function

### 4.4.1 Using $\beta$ as a scaling parameter

Defining the nondimensional radius in the same way that SWIRL does:

$$\tilde{r} = \frac{r}{r_T}$$

where  $r_T$  is the outer radius of the annulus.

The hub-to-tip ratio is defined as:

$$\sigma = \frac{r_H}{r_T} = \tilde{r}_H$$

where  $\tilde{r}_H$  is the inner radius of the annular duct. The hub-to-tip ratio can also be zero indicating the duct is hollow.

A useful and similar parameter is introduced,  $\beta$ , where  $0 \leq \beta \leq 1$

$$\beta = \frac{r - r_H}{r_T - r_H}$$



Dividing By  $r_T$

$$\begin{aligned}\beta &= \frac{\frac{r}{r_T} - \frac{r_H}{r_T}}{\frac{r_T}{r_T} - \frac{r_H}{r_T}} \\ &= \frac{\tilde{r} - \tilde{r}_H}{1 - \sigma}\end{aligned}$$

Suppose a manufactured solution  $f_{MS}$  with boundaries  $f_{MS}(r = \sigma)$  and  $f_{MS}(\tilde{r} = 1)$  is the specified analytical solution. The goal is to change the boundary conditions of the manufactured solution in such way that allows us to adequately check the boundary conditions imposed on SWIRL. Defining the manufactured solution,  $f_{MS}(\tilde{r})$ , where  $\sigma \leq \tilde{r} \leq 1$  and there are desired values of  $f$  at the boundaries desired values are going to be denoted as  $f_{minBC}$  and  $f_{maxBC}$ . The desired changes in  $f$  are defined as:

$$\begin{aligned}\Delta f_{minBC} &= f_{minBC} - f_{MS}(\tilde{r} = \sigma) \\ \Delta f_{maxBC} &= f_{maxBC} - f_{MS}(\tilde{r} = 1)\end{aligned}$$

We'd like to impose these changes smoothly on the manufactured solution function. To do this, the fairing functions,  $A_{min}(\tilde{r})$  and  $A_{max}(\tilde{r})$  where:

$$f_{BCsImposed}(\tilde{r}) = f_{MS}(\tilde{r}) + A_{min}(\tilde{r})\Delta f_{minBC} + A_{max}(\tilde{r})\Delta f_{maxBC}$$

Then, in order to set the condition at the appropriate boundary, the following conditions are set,

$$A_{min}(\tilde{r} = \sigma) = 1$$

$$A_{min}(\tilde{r} = 1) = 0$$

$$A_{max}(\tilde{r} = 1) = 1$$

$$A_{max}(\tilde{r} = \sigma) = 0$$

If  $A_{min}(\tilde{r})$  is defined as a function of  $A_{max}(\tilde{r})$  then only  $A_{max}(\tilde{r})$  needs to be defined, therefore

$$A_{min}(\tilde{r}) = 1 - A_{max}(\tilde{r})$$

It is also desirable to set the derivatives for the fairing function at the boundaries incase there are boundary conditions imposed on the derivatives of the fairing function.

$$\frac{\partial A_{max}}{\partial \tilde{r}}|_{\tilde{r}=\sigma} = 0$$

$$\frac{\partial A_{max}}{\partial \tilde{r}}|_{\tilde{r}=1} = 0$$

$$\frac{\partial A_{min}}{\partial \tilde{r}}|_{\tilde{r}=\sigma} = 0$$

$$\frac{\partial A_{min}}{\partial \tilde{r}}|_{\tilde{r}=1} = 0$$

#### 4.4.2 Minimum Boundary Fairing Function

Looking at  $A_{min}$  first, the polynomial is:

$$A_{min}(\beta) = a + b\beta + c\beta^2 + d\beta^3$$

$$A_{min}(\tilde{r}) = a + b\left(\frac{\tilde{r} - \sigma}{1 - \sigma}\right) + c\left(\frac{\tilde{r} - \sigma}{1 - \sigma}\right)^2 + d\left(\frac{\tilde{r} - \sigma}{1 - \sigma}\right)^3$$

Taking the derivative,

$$A'_{min}(\tilde{r}) = b\left(\frac{1}{1 - \sigma}\right) + 2c\left(\frac{1}{1 - \sigma}\right)\left(\frac{\tilde{r} - \sigma}{1 - \sigma}\right) + 3d\left(\frac{1}{1 - \sigma}\right)\left(\frac{\tilde{r} - \sigma}{1 - \sigma}\right)^2$$

$$A'_{min}(\beta) = \left(\frac{1}{1 - \sigma}\right)[b + 2c\beta + 3d\beta^2]$$

Now we will use the conditons mentioned earlier as constraints to this system of equations Using the possible values of  $\tilde{r}$ ,

$$A_{min}(\sigma) = a \qquad \qquad \qquad = 1$$

$$A_{min}(1) = a + b + c + d \qquad \qquad \qquad = 0$$

$$A'_{min}(\sigma) = b \qquad \qquad \qquad = 0$$

$$A'_{min}(1) = b + 2c + 3d \qquad \qquad \qquad = 0$$

which has the solution,

$$a = 1$$

$$b = 0$$

$$c = -3$$

$$d = 2$$

giving the polynomial as:

$$A_{min}(\tilde{r}) = 1 - 3 \left( \frac{\tilde{r} - \sigma}{1 - \sigma} \right)^2 + 2 \left( \frac{\tilde{r} - \sigma}{1 - \sigma} \right)^3$$

#### 4.4.3 Max boundary polynomial

Following the same procedure for  $A_{max}$  gives

$$A_{min}(\tilde{r}) = 3 \left( \frac{\tilde{r} - \sigma}{1 - \sigma} \right)^2 - 2 \left( \frac{\tilde{r} - \sigma}{1 - \sigma} \right)^3$$

#### 4.4.4 Corrected function

The corrected function is then,

$$\begin{aligned} f_{BCsImposed}(\tilde{r}) &= f_{MS}(\tilde{r}) + A_{min}\Delta f_{minBC} + A_{max}\Delta f_{maxBC} \\ &= f_{MS}(\tilde{r}) + \left( 1 - 3 \left( \frac{\tilde{r} - \sigma}{1 - \sigma} \right)^2 + 2 \left( \frac{\tilde{r} - \sigma}{1 - \sigma} \right)^3 \right) [\Delta f_{minBC}] \\ &\quad + \left( 3 \left( \frac{\tilde{r} - \sigma}{1 - \sigma} \right)^2 - 2 \left( \frac{\tilde{r} - \sigma}{1 - \sigma} \right)^3 \right) [\Delta f_{maxBC}] \\ f_{BCsImposed}(\beta) &= f_{MS}(\beta) + \Delta f_{minBC} + (3\beta^2 - 2\beta^3) [\Delta f_{maxBC} - \Delta f_{minBC}] \end{aligned}$$

Note that we're carrying the correction throughout the domain, as opposed to limiting the correction at a certain distance away from the boundary. The application of this correction ensures that there is no discontinuous derivatives inside the domain; as suggested in Roach's MMS guidelines (insert ref)

What is meant by “just because  $A_{min}$  and its first derivative go to zero doesn't mean that the second derivatives”

#### 4.4.5 Symbolic Sanity Checks

We want to ensure that  $f_{BCsImposed}$  has the desired boundary conditions,  $f_{minBC/maxBC}$  instead of the original boundary values that come along for the ride in the manufactured solutions,  $f_{MS}(\tilde{r} = \sigma/1)$ . In another iteration of this method, we will be changing the derivative values, so let's check the values of  $\frac{\partial f_{BCsImposed}}{\partial \tilde{r}}$  to make sure those aren't effected unintentionally.

##### Symbolic Sanity Check 1

The modified manufactured solution,  $f_{BCsImposed}$  with the fairing functions  $A_{min}$  and  $A_{max}$  substituted in is,

$$f_{BCsImposed}(\tilde{r}) = \left( 3 \left( \frac{\tilde{r} - \sigma}{1 - \sigma} \right)^2 - 2 \left( \frac{\tilde{r} - \sigma}{1 - \sigma} \right)^3 \right) [\Delta f_{maxBC}].$$

Further simplification yields,

$$\begin{aligned} f_{BCsImposed}(\tilde{r} = \sigma) &= \left( f_{MS}(\tilde{r} = \sigma) + \Delta f_{minBC} + \left( 3 \left( \frac{\sigma - \sigma}{1 - \sigma} \right)^2 - 2 \left( \frac{\sigma - \sigma}{1 - \sigma} \right)^3 - \right) [\Delta f_{maxBC} - \Delta f_{minBC}] \right) \\ &= f_{MS}(\tilde{r} = \sigma) + \Delta f_{minBC} \\ &= f_{MS}(\tilde{r} = \sigma) + (f_{minBC} - f_{MS}(\tilde{r} = \sigma)) \\ &= f_{minBC} \end{aligned}$$

$$\begin{aligned}
f_{BCsImposed}(\tilde{r} = 1) &= \left( f_{MS}(\tilde{r} = 1) + \Delta f_{minBC} + \left( 3 \left( \frac{1-\sigma}{1-\sigma} \right)^2 - 2 \left( \frac{1-\sigma}{1-\sigma} \right)^3 - \right) [\Delta f_{maxBC} - \Delta f_{minBC}] \right) \\
&= f_{MS}(\tilde{r} = 1) + \Delta f_{maxBC} \\
&= f_{MS}(\tilde{r} = 1) + (f_{maxBC} - f_{MS}(\tilde{r} = 1)) \\
&= f_{maxBC}
\end{aligned}$$

$$\begin{aligned}
&\frac{\partial}{\partial \tilde{r}} \left( f_{BCsImposed}(\tilde{r}) = \left( 3 \left( \frac{\tilde{r}-\sigma}{1-\sigma} \right)^2 - 2 \left( \frac{\tilde{r}-\sigma}{1-\sigma} \right)^3 \right) [\Delta f_{maxBC}] \right) \\
&\frac{\partial f_{MS}}{\partial \tilde{r}} + \left( \frac{6}{1-\sigma} \right) \left( \left( \frac{\tilde{r}-\sigma}{1-\sigma} \right) - \left( \frac{\tilde{r}-\sigma}{1-\sigma} \right)^2 \right) (\Delta f_{maxBC} - \Delta f_{minBC})
\end{aligned}$$

At  $\tilde{r} = \sigma$ , the derivative is:

$$\begin{aligned}
&\frac{\partial f_{MS}}{\partial \tilde{r}}|_{\sigma} \\
&\frac{\partial f_{MS}}{\partial \tilde{r}}|_1
\end{aligned}$$

#### 4.4.6 Min boundary derivative polynomial

The polynomial is of the form:

$$\begin{aligned}
B_{min}(\beta) &= a + b\beta + c\beta^2 + d\beta^3 \\
B_{min}(\tilde{r}) &= a + b \left( \frac{\tilde{r}-\sigma}{1-\sigma} \right) + c \left( \frac{\tilde{r}-\sigma}{1-\sigma} \right)^2 + d \left( \frac{\tilde{r}-\sigma}{1-\sigma} \right)^3
\end{aligned}$$

Taking the derivative,

$$B'_{min}(\tilde{r}) = b \left( \frac{1}{1-\sigma} \right) + 2c \left( \frac{1}{1-\sigma} \right) \left( \frac{\tilde{r}-\sigma}{1-\sigma} \right) + 3d \left( \frac{1}{1-\sigma} \right) \left( \frac{\tilde{r}-\sigma}{1-\sigma} \right)^2$$

$$B'_{min}(\beta) = \left( \frac{1}{1-\sigma} \right) [b + 2c\beta + 3d\beta^2]$$

Applying the four constraints gives:

$$a = 0$$

$$b = (1 - \sigma)$$

$$a + b + c + d = 0$$

$$2 + 2c + 3d = 0$$

$$c + d = -b$$

$$2c + 3d = -b$$

$$c = -2b$$

$$d = b$$

and the min boundary derivative polynomial is:

$$B_{min}(\tilde{r}) = b \left( \frac{\tilde{r}-\sigma}{1-\sigma} \right) - 2b \left( \frac{\tilde{r}-\sigma}{1-\sigma} \right)^2 + b \left( \frac{\tilde{r}-\sigma}{1-\sigma} \right)^3$$

$$= (1 - \sigma) \left( \left( \frac{\tilde{r}-\sigma}{1-\sigma} \right) - 2 \left( \frac{\tilde{r}-\sigma}{1-\sigma} \right)^2 + \left( \frac{\tilde{r}-\sigma}{1-\sigma} \right)^3 \right)$$

#### 4.4.7 Polynomial function, max boundary derivative

The polynomial is of the form:

The polynomial is of the form:

$$B_{max}(\beta) = a + b\beta + c\beta^2 + d\beta^3$$

$$B_{max}(\tilde{r}) = a + b\left(\frac{\tilde{r} - \sigma}{1 - \sigma}\right) + c\left(\frac{\tilde{r} - \sigma}{1 - \sigma}\right)^2 + d\left(\frac{\tilde{r} - \sigma}{1 - \sigma}\right)^3$$

which has the derivative,

$$B'_{max}(\tilde{r}) = b\left(\frac{1}{1 - \sigma}\right) + 2c\left(\frac{1}{1 - \sigma}\right)\left(\frac{\tilde{r} - \sigma}{1 - \sigma}\right) + 3d\left(\frac{1}{1 - \sigma}\right)\left(\frac{\tilde{r} - \sigma}{1 - \sigma}\right)^2$$

$$B'_{max}(\beta) = \left(\frac{1}{1 - \sigma}\right)[b + 2c\beta + 3d\beta^2]$$

Applying the four constraints gives:

$$a = 0$$

$$b = 0$$

$$a + b + c + d = 0$$

$$b + 2c + 3d = (1 - \sigma)$$

working this out:

$$c + d = 0$$

$$2c + 3d = (1 - \sigma)$$

gives



$$c = -(1 - \sigma) d = (1 - \sigma)$$

and the max boundary derivative polynomial is:

$$B_{max}(\tilde{r}) = (1 - \sigma) \left( - \left( \frac{\tilde{r} - \sigma}{1 - \sigma} \right)^2 + \left( \frac{\tilde{r} - \sigma}{1 - \sigma} \right)^3 \right)$$

#### 4.4.8 Putting it together

The corrected function is then:

$$\begin{aligned} f_{BCsImposed}(\tilde{r}) &= f_{MS} + B_{min}(\tilde{r}) \Delta f'_{minBC} + B_{max}(\tilde{r}) \Delta f'_{maxBC} \\ &= f_{MS} + \\ &\quad (1 - \sigma) \left( \left( \frac{\tilde{r} - \sigma}{1 - \sigma} \right) - \left( \frac{\tilde{r} - \sigma}{1 - \sigma} \right)^2 \right) \Delta f'_{minBC} + \\ &\quad (1 - \sigma) \left( - \left( \frac{\tilde{r} - \sigma}{1 - \sigma} \right)^2 + \left( \frac{\tilde{r} - \sigma}{1 - \sigma} \right)^3 \right) (\Delta f'_{minBC} + \Delta f'_{maxBC}) \end{aligned}$$

# Chapter 5

## Results and Discussion

### 5.1 Verification of Numerical Schemes using the Method of Manufactured Solution

#### 5.1.1 Introduction

The frequency domain, linearized Euler equation computer code, SWIRL, was verified through the Methods of Manufactured and Exact solutions. However, while the Method of Exact Solutions (MES) can be used to validate the output of SWIRL, there is a limitation on the number of exact solutions available based on the flow and domain. Any changes in a flow configuration (uniform axial flow vs. sheared axial flow, without any tangential component) require a recalculation of the analytical solution. Code validation through MES is for the case of uniform flow in a cylindrical duct since the exact solution requires implementing special Bessel functions. In addition, the exact solution needs to be recomputed for changes in radii and the use of acoustic liner (i.e., boundary conditions). For this reason, the more comprehensive MMS was first used for code verification to test each variable in the governing equations and gain measurable acceptance criteria without relying on expert judgment.

MMS was implemented on a component level since SWIRL consists of two main

numerical approximations for flows with axial and tangential components. First, the numerical integration technique required for radial change in sound speed was verified. Then, the four governing equations that make up the matrices required for the eigenvalue problem were tested. Note that the output of the eigenvalue problem was tested with MMS by recomputing the expression  $[A]x - \lambda[B]x = 0$  with a given eigenvalue/vector pair. The calculated  $L_{2,norm}$  (i.e. error and the order of accuracy for both numerical methods are discussed below. The MMS was then used to compare against validation cases in literature to outline the methodology for test cases for which there is no solution.

### 5.1.2 MMS, Solutions

(insert table instead of equations, check comments in tex file for parameters)

$$M_x = 0.3 \left( \sum_{j=1}^5 R_{ij} + \sum_{j=1}^5 L_{ij} + 1 \right), B = 50 \quad (5.1)$$

$$\tilde{A} = \left( \sum_{j=1}^5 R_{ij} + \sum_{j=1}^5 L_{ij} + 1 \right), B = 0.3 \quad (5.2)$$

$$\tilde{v}_{r,BCsImposed} = \sum_{j=1}^3 R_{ij} + \sum_{j=1}^3 L_{ij} + 1, \quad (5.3)$$

$$B = 2, \quad (5.4)$$

$$\tilde{v}_{r,BCsImposed}(\tilde{r}_{min} = \tilde{r}_{max}) = 0 \quad (5.5)$$

$$\tilde{v}_{\theta} = \left( \sum_{j=1}^4 R_{ij} + \sum_{j=1}^4 L_{ij} + 1 \right), B = 50 \quad (5.6)$$

$$\tilde{v}_x = \sum_{j=1}^3 R_{ij} + \sum_{j=1}^3 L_{ij} + 1, B = 30 \quad (5.7)$$

$$\tilde{p}_{diffBCsImposed} = \sum_{j=1}^5 R_{ij} + \sum_{j=1}^5 L_{ij} + 1, B = 30 \quad (5.8)$$

Figure 5-1 shows the manufactured solution for the mean flow profile. The tangent summation method was used to generate the axial Mach number, the speed of sound, and the perturbation variables. The tangential Mach number was numerically approximated by using the composite trapezoidal rule. The manufactured mean flow profile is unique because it has been generated solely to verify SWIRL and does not have physical significance. The “kinks” in the solution will allow a significant magnitude for the derivatives of these solutions.

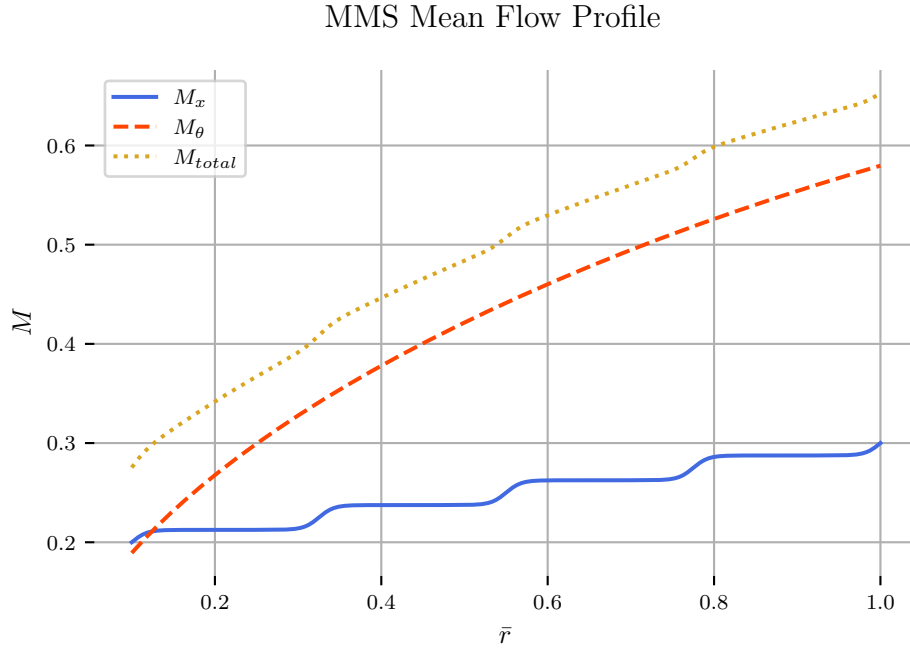


Figure 5-1: The manufactured mean flow test case using a summation of Tangents for  $A$  and  $M_x$

The results from the numerical integration are presented in Figure 5-2. Although

the slope of the line appears linear, the TSM was still used to generate the MS for the speed of sound. Denser grids were used to compute the error by iterating as grid spacing approaches zero. The difference between the expected speed of sound to the actual speed of sound is shown in Figure 5-3 as a function of radius. Note that the error reaches machine precision early in the iterations and approaches zero as more grid points are used.

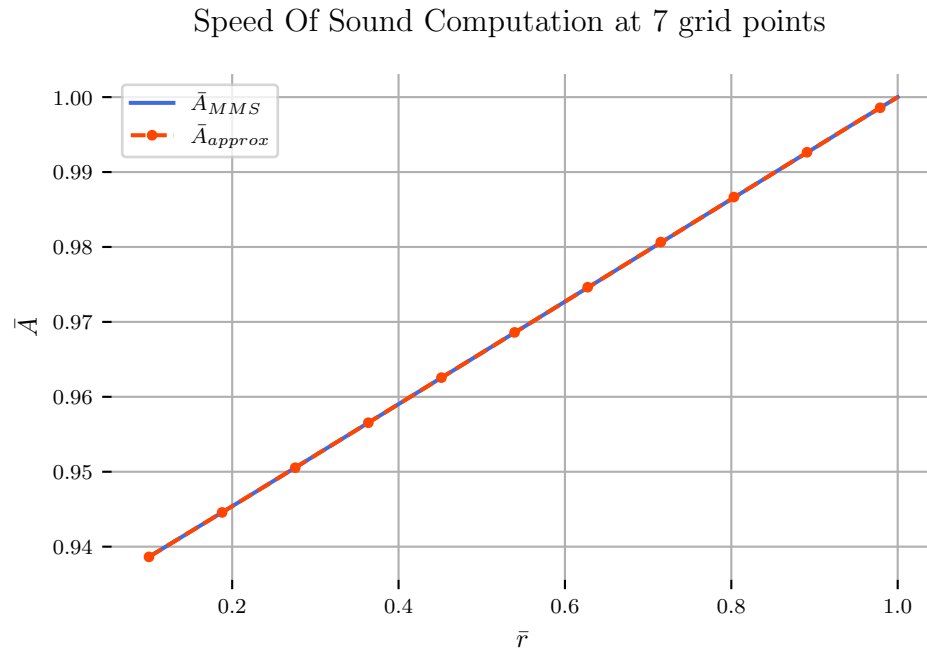


Figure 5-2: A comparison of the speed of sound, expected vs actual at the lowest grid to show similarities in solution

The error will decrease at a known rate depending on the type of numerical integration scheme. Since the composite trapezoidal rule has an order of accuracy of 2, it is expected that the approximated order of accuracy will approach two as the error approaches zero. This behavior is shown in Figure 5-4, where the approximated line is the L2 norm of the speed of sound error. The slope (i.e., the asymptotic rate of convergence) approached two for numerical integration as the grid spacing decreases (See Figure 5.1.2) .

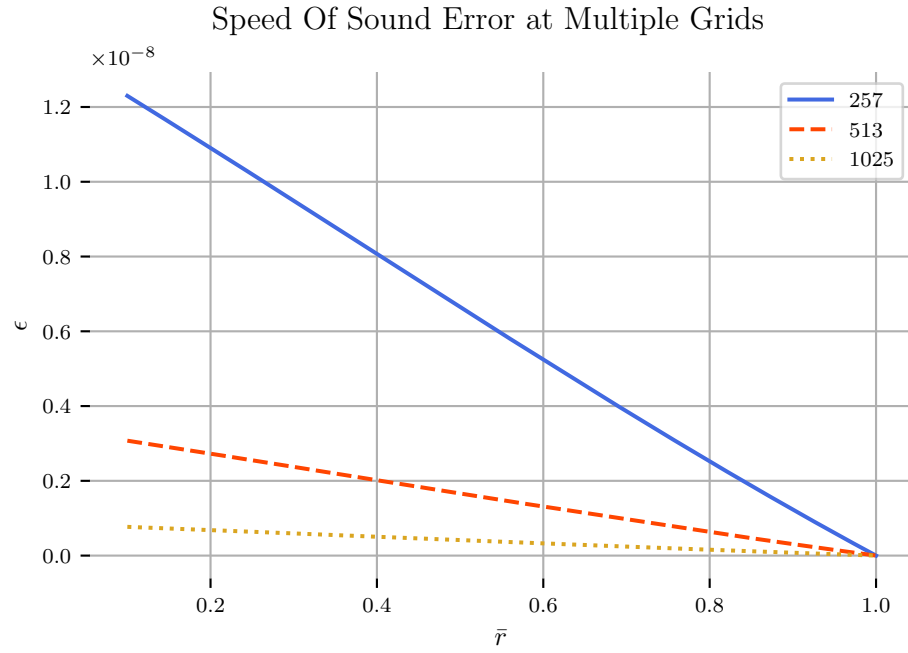


Figure 5-3: A comparison of the speed of sound error at three grid

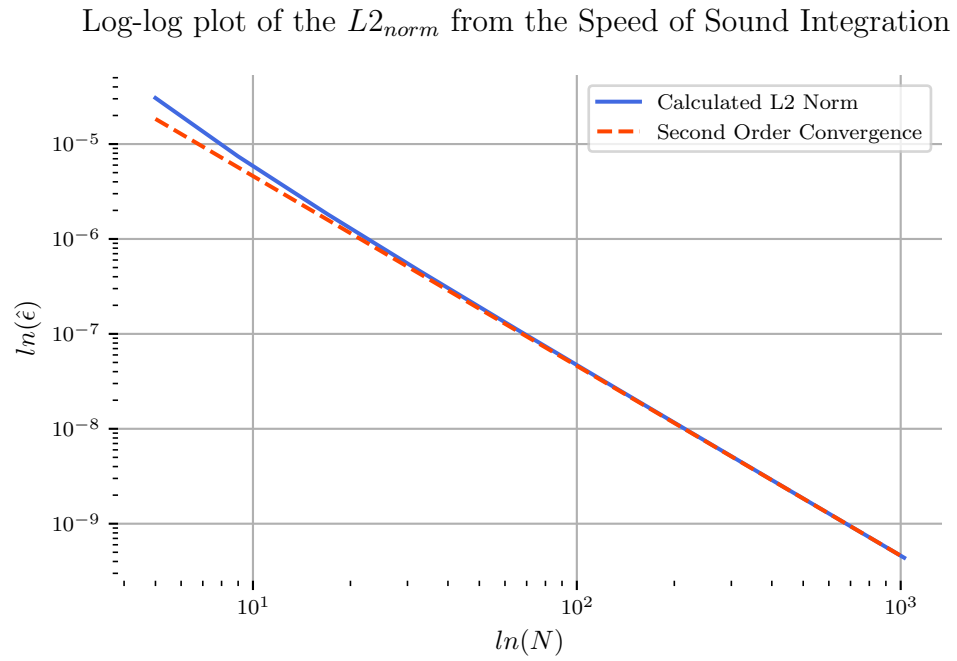


Figure 5-4: L2 Norm comparison for the speed of sound integration for the compound trapezoidal rule

The manufactured solution used for the fluctuation variables in the MMS test case is shown in Table ?? . Recall that the variable  $B$  varies the slope around the tangent function at each inflection point; the maximum amplitude of each tangent function was  $A = 0.1$  and was equally spaced between  $\tilde{r}_{min}$ - $\tilde{r}_{max}$ . The boundary conditions for the perturbation variable  $\tilde{v}_r$  were set using the fairing functions to impose boundary conditions. Fairing functions also set the derivative of the perturbation variable  $\tilde{p}$ . Only  $\tilde{p}$  is affected by acoustic liners since it alters the rate of change of pressure at the walls, not the pressure or velocity. The subscripts *BCsImposed*, *diffBCsImposed* state where the perturbation or its derivative value was altered to be uniform between the code and the manufactured solution.

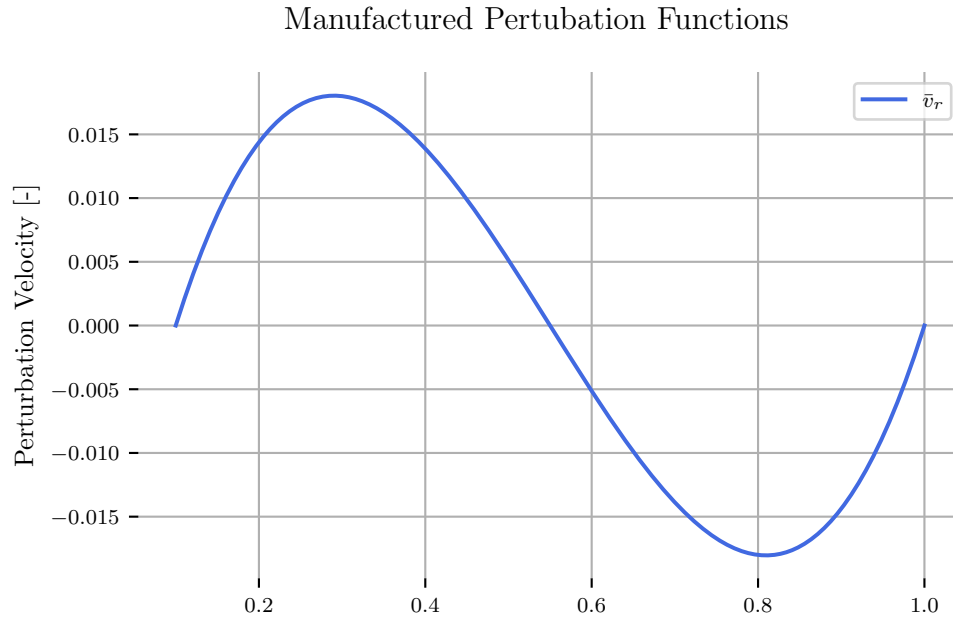


Figure 5-5: The manufactured perturbation functions , $v_r$

A second and fourth-order central differencing scheme for the LEE is used for the approximated radial derivatives and compared to the source terms generated for the MMS in Figure 5-10. The L2 norm and the asymptotic rate of convergence is shown for the two differencing schemes in 5-15 .

### Manufactured Pertubation Functions

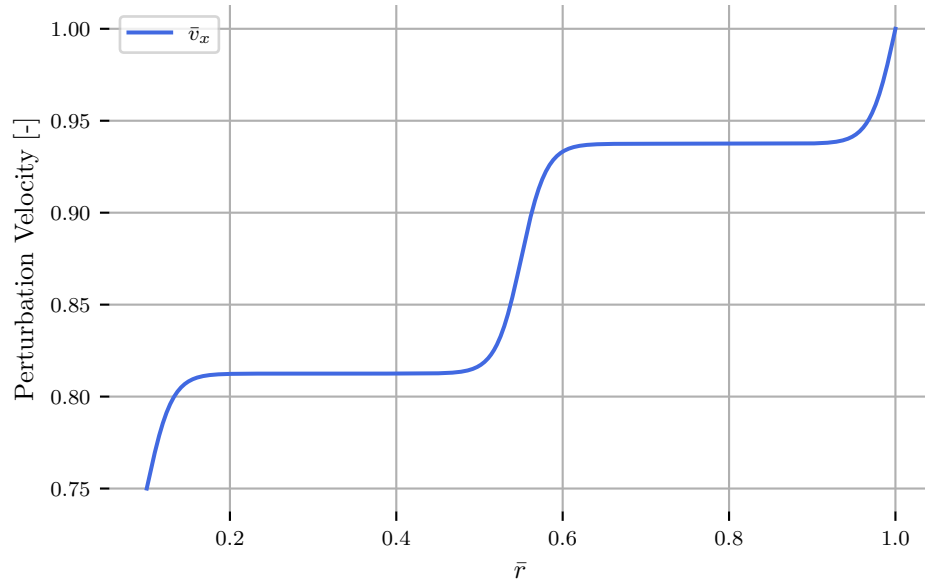


Figure 5-6: The manufactured perturbation functions , $v_x$

### Manufactured Pertubation Functions

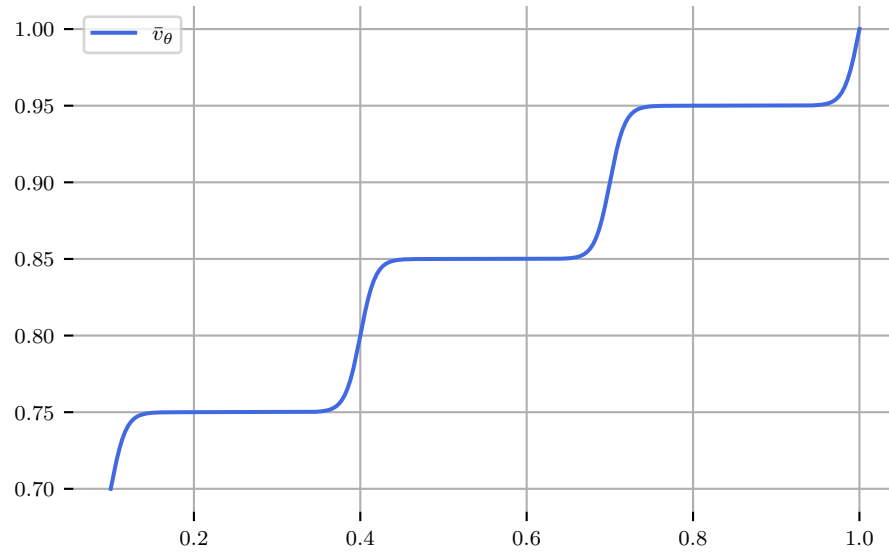


Figure 5-7: The manufactured perturbation functions , $v_\theta$

The grid points were doubled, starting at 7 grid points and ending after 9 iterations with 1025 grid points. Both schemes do not have the order of accuracy down to



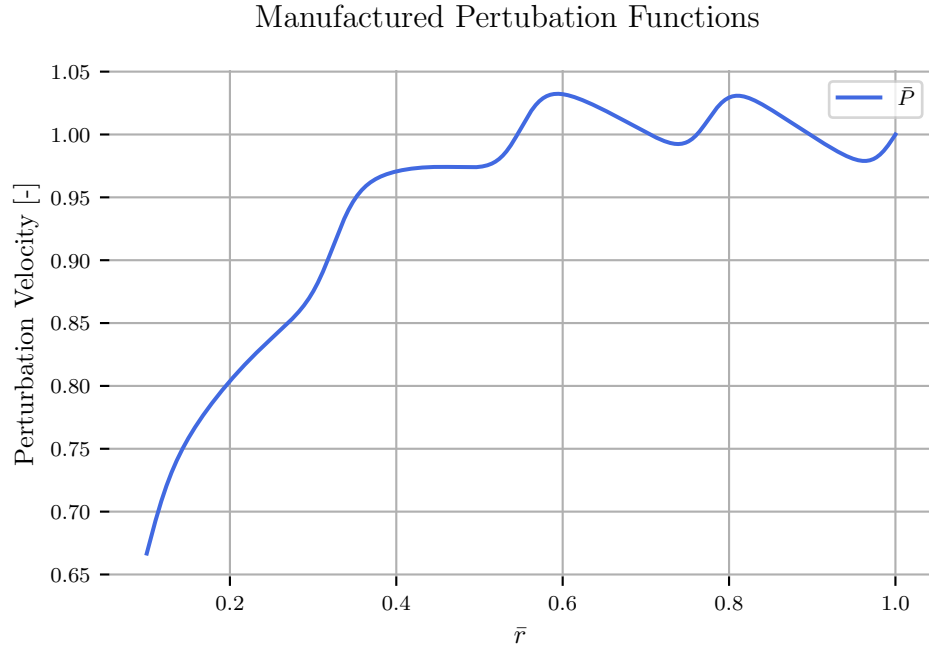


Figure 5-8: The manufactured perturbation functions , $\bar{P}$

machine precision but get down to  $10^{-6}$  For the LEE, a second and fourth order central differencing scheme is used for the approximated radial derivatives and then compared to the source terms generated for the MMS in Figure 5-10.

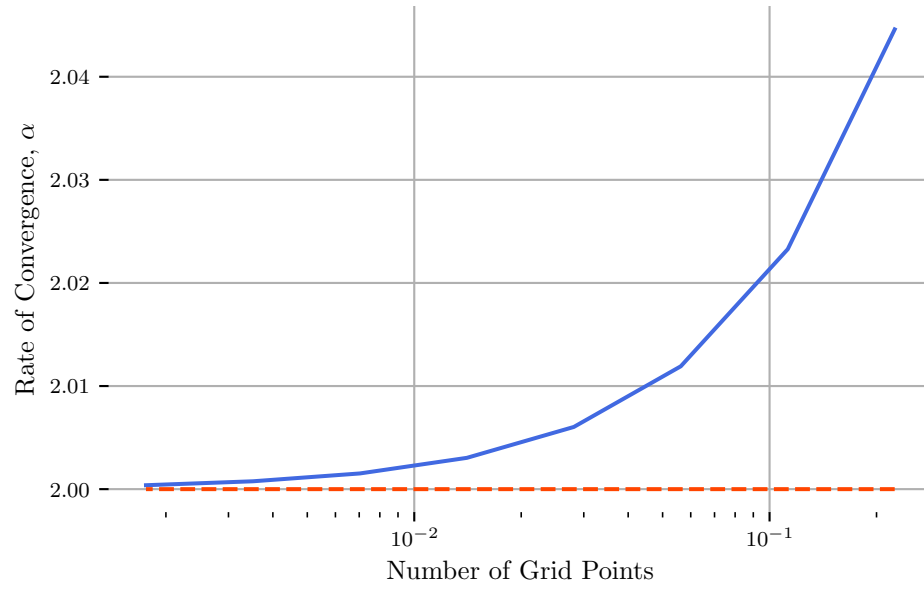


Figure 5-9: Speed of Sound Rate Of Convergence

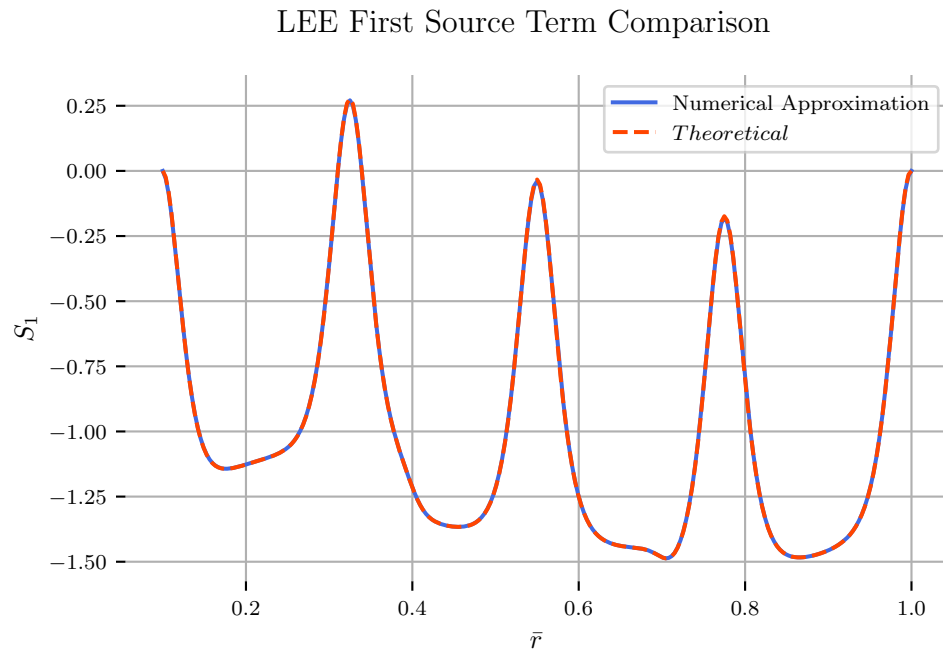


Figure 5-10: Comparison of manufactured source term for the first linearized Euler equation

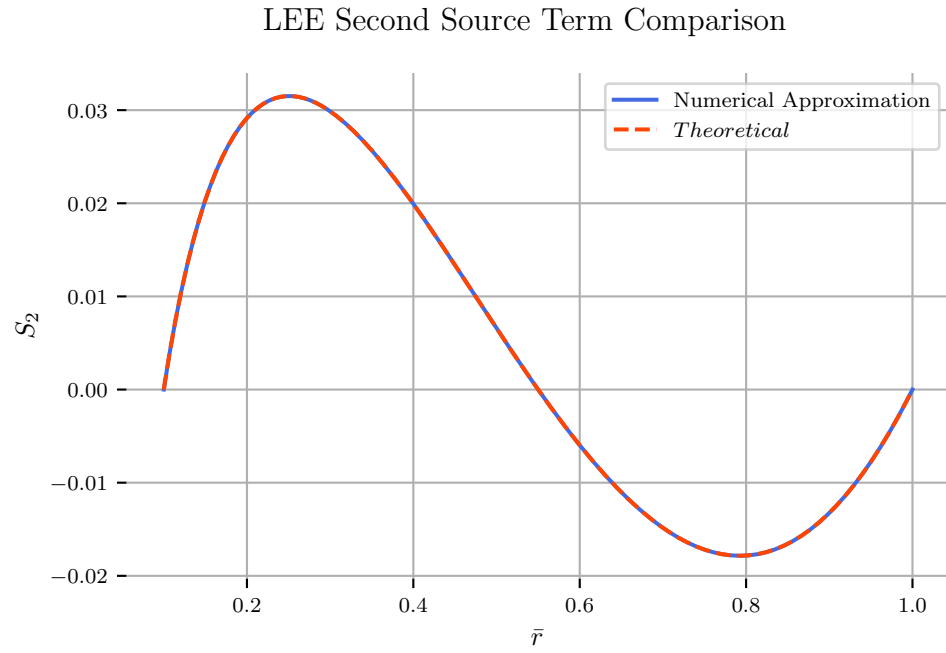


Figure 5-11: Comparison of manufactured source term for the second linearized Euler equation

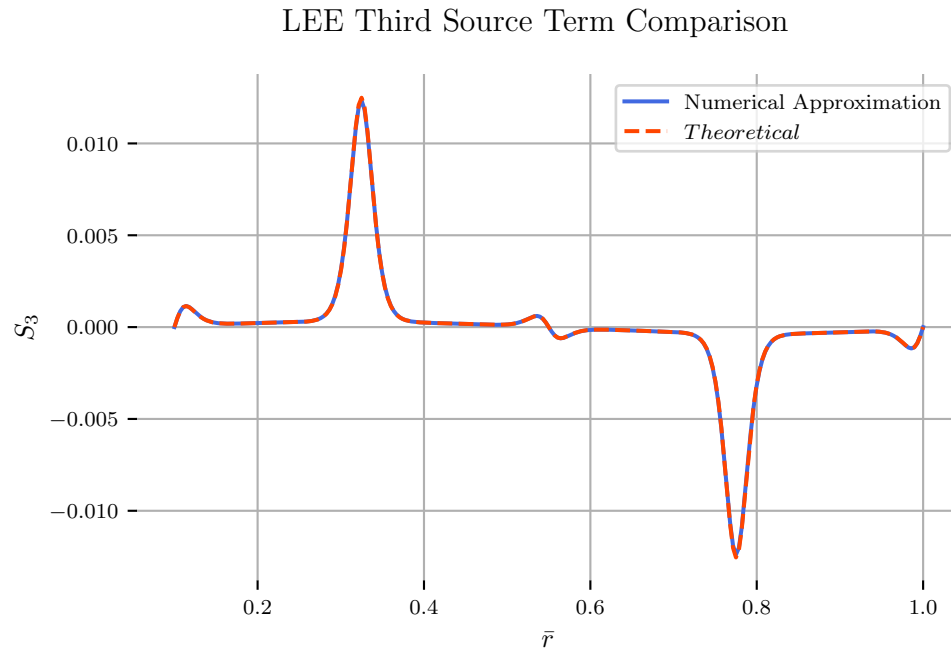


Figure 5-12: Comparison of manufactured source term for the third linearized Euler equation

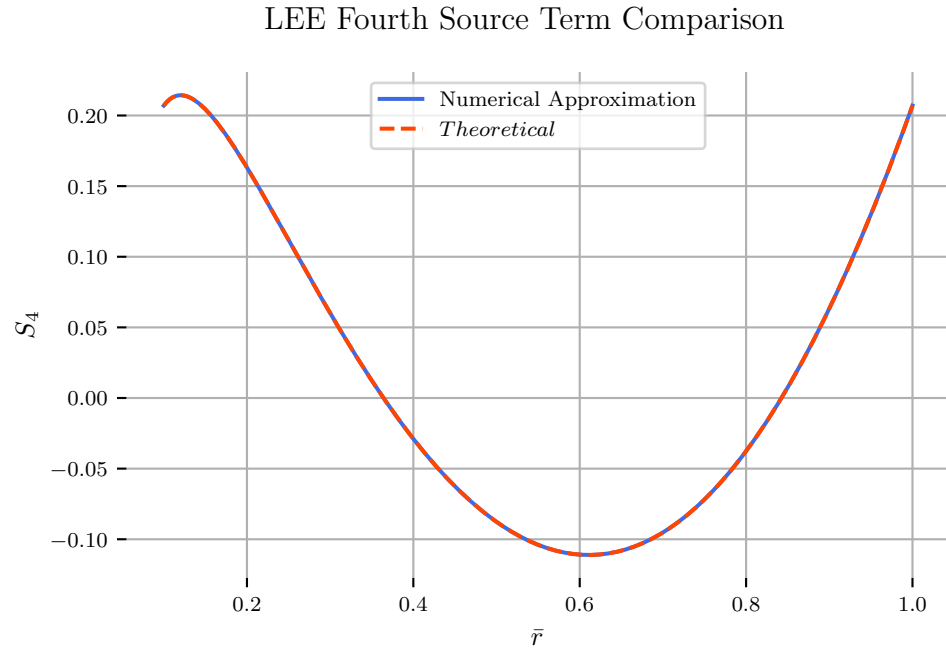


Figure 5-13: Comparison of manufactured source term for the fourth linearized Euler equation

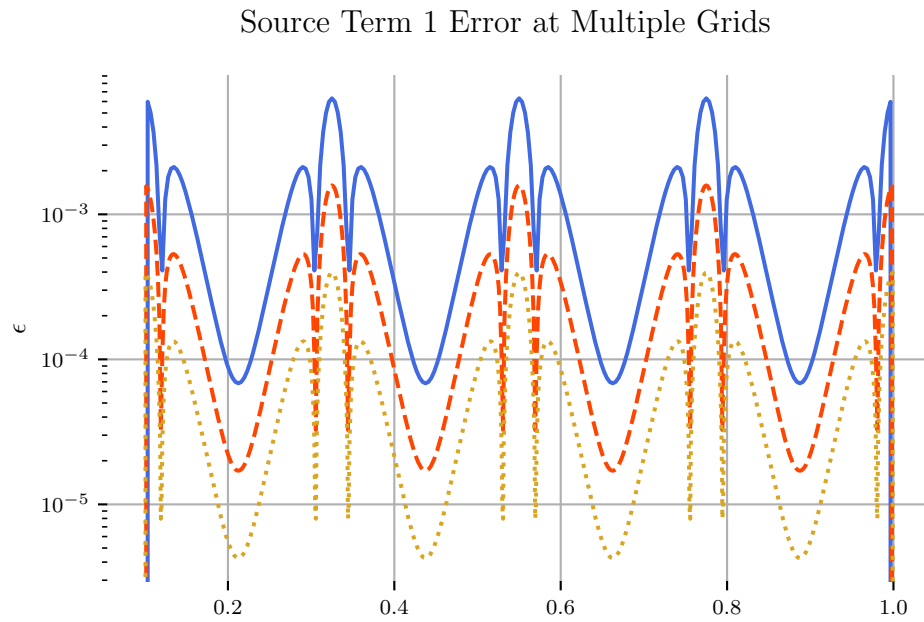


Figure 5-14: LEE Source Term Error

Source Term 2 Error at Multiple Grids

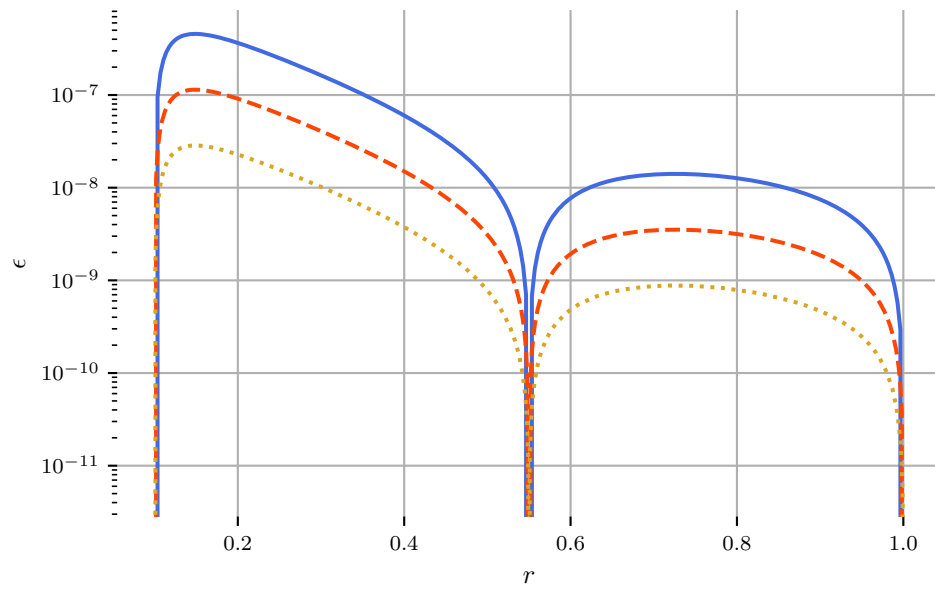


Figure 5-15: LEE Source Term Error

Source Term 3 Error at Multiple Grids

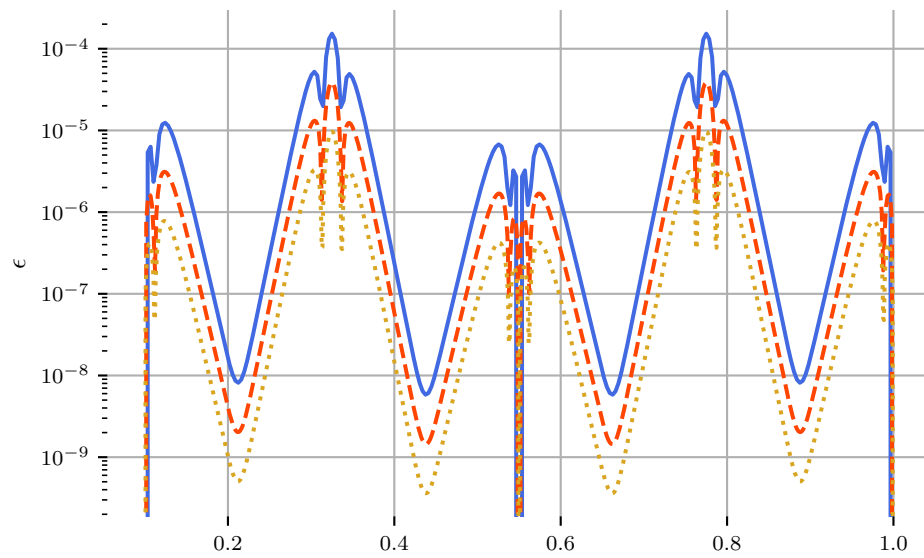


Figure 5-16: LEE Source Term Error

Source Term 4 Error at Multiple Grids

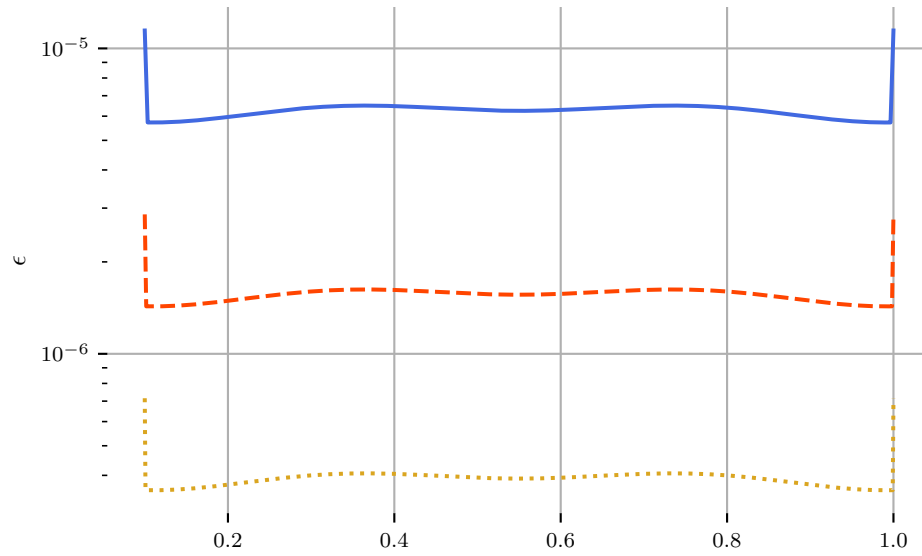
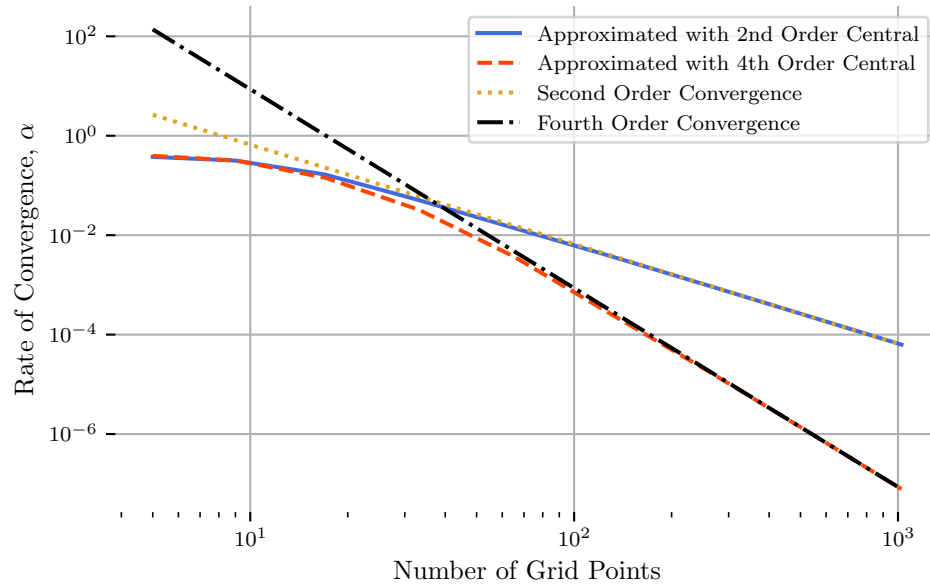
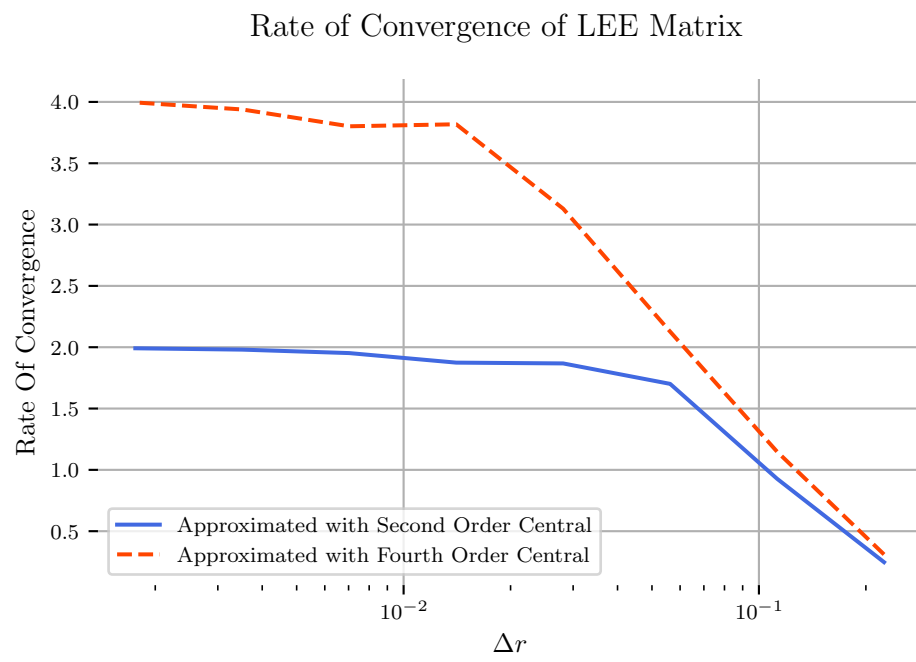


Figure 5-17: LEE Source Term Error

L2 of LEE Matrix





# References

- [1] Small-amplitude disturbances in turbomachine flows with swirl - david w. wundrow - google books.
- [2] Chapter 3 exact methods of solution. *Mathematics in Science and Engineering*, 18:71–122, 1 1965.
- [3] *INDEPENDENT EXPERT INTEGRATED TECHNOLOGY GOALS ASSESSMENT AND REVIEW FOR ENGINES AND AIRCRAFT REPORT*. 2019.
- [4] Department Of Transportation Federal Aviation Administration. Aviation environmental and energy policy statement - july 2012, 2012.
- [5] N. K. Agarwal and M. K. Bull. Acoustic wave propagation in a pipe with fully developed turbulent flow. *Journal of Sound and Vibration*, 132:275–298, 7 1989.
- [6] R. J. Astley and W. Eversman. A finite element formulation of the eigenvalue problem in lined ducts with flow. *Journal of Sound and Vibration*, 65:61–74, 7 1979.
- [7] K. M. Case. Stability of inviscid plane couette flow. *The Physics of Fluids*, 3:143, 11 2004.
- [8] A. J. Cooper. Effect of mean entropy on unsteady disturbance propagation in a slowly varying duct with mean swirling flow. *Journal of Sound and Vibration*, 291:779–801, 4 2006.



- [9] A. J. COOPER and N. PEAKE. Propagation of unsteady disturbances in a slowly varying duct with mean swirling flow. *Journal of Fluid Mechanics*, 445:207–234, 10 2001.
- [10] Edmane Envia, Alexander G. Wilson, and Dennis L. Huff. Fan noise: A challenge to caa, 8 2004.
- [11] M. E. Goldstein. Characteristics of the unsteady motion on transversely sheared mean flows. *Journal of Fluid Mechanics*, 84:305, 1 1978.
- [12] M. E. Goldstein. Scattering and distortion of the unsteady motion on transversely sheared mean flows. *Journal of Fluid Mechanics*, 91:601–632, 1979.
- [13] V. V. Golubev and H. M. Atassi. Acoustic-vorticity waves in swirling flows. *Journal of Sound and Vibration*, 209:203–222, 1 1998.
- [14] Vladimir V. Golubev and Hafiz M. Atassi. Acoustic-vorticity modes in an annular duct with mean vortical swirling flow. *3rd AIAA/CEAS Aeroacoustics Conference*, pages 804–814, 1997.
- [15] VV Golubev and HM Atassi. Sound propagation in an annular duct with mean potential swirling flow. *Journal of Sound and Vibration*, 198(5):601–616, 1996.
- [16] Ying Guan, Kai H. Luo, and Tong Q. Wang. Sound transmission in a lined annular duct with mean swirling flow. *American Society of Mechanical Engineers, Noise Control and Acoustics Division (Publication) NCAD*, pages 135–144, 6 2009.
- [17] C. J. Heaton and N. Peake. Algebraic and exponential instability of inviscid swirling flow. *Journal of Fluid Mechanics*, 565:279–318, 10 2006.

- [18] Ray Hixon, Adrian Sescu, and Vasanth Allampalli. Towards the prediction of noise from realistic rotor wake/stator interaction using caa. volume 6, pages 203–213. Elsevier Ltd, 2010.
- [19] Daniel Ingraham. Verification of a computational aeroacoustics code using external verification analysis (eva), 2010.
- [20] Daniel Ingraham and Ray Hixon. Verification of a viscous computational aeroacoustics code using external verification analysis aiaa paper 2015-2225 motivation.
- [21] A. KAPUR and P. MUNGUR. Sound interaction with a helical flow contained in an annular duct with radial gradients of flow, density and temperature. 1973.
- [22] J. L. KERREBROCK. Waves and wakes in turbomachine annuli with swirl. 1974.
- [23] J. L. Kerrebrock. Small disturbances in turbomachine annuli with swirl. <https://doi.org/10.2514/3.7370>, 15:794–803, 5 2012.
- [24] Jack L. Kerrebrock. *Aircraft engines and gas turbines*. MIT Press, 1992.
- [25] Kenneth Kousen. Pressure modes in ducted flows with swirl. In *Aeroacoustics Conference*, page 1679, 1996.
- [26] Kenneth A Kousen. Eigenmode analysis of ducted flows with radially dependent axial and swirl components. In *CEAS/AIAA Joint Aeroacoustics Conference, 1st, Munich, Germany*, pages 1085–1094, 1995.
- [27] Konrad Kozaczuk. Engine nacelles design – problems and challenges. *Proceedings of the Institution of Mechanical Engineers, Part G: Journal of Aerospace Engineering*, 231:2259–2265, 10 2017.

- [28] A. L.P. Maldonado, R. J. Astley, J. Coupland, G. Gabard, and D. Sutliff. Sound propagation in lined annular ducts with mean swirling flow. American Institute of Aeronautics and Astronautics Inc, AIAA, 2016.
- [29] Ronald Nijboer. Eigenvalues and eigenfunctions of ducted swirling flows. *7th AIAA/CEAS Aeroacoustics Conference and Exhibit*, 2001.
- [30] H. Posson and N. Peake. The acoustic analogy in an annular duct with swirling mean flow. *Journal of Fluid Mechanics*, 726:439–475, 2013.
- [31] Christopher J. Roy. Review of code and solution verification procedures for computational simulation. *Journal of Computational Physics*, 205:131–156, 5 2005.
- [32] Kambiz Salari and Patrick Knupp. Code verification by the method of manufactured solutions, 2000.
- [33] P N Shankar. Acoustic refraction and attenuation in cylindrical and annular ducts, 1972.
- [34] Michael JT Smith. Aircraft noise. *Cambridge Aerospace Series*, 1989.
- [35] Christopher K.W. Tam and Laurent Auriault. The wave modes in ducted swirling flows. *Journal of Fluid Mechanics*, 371:1–20, 9 1998.
- [36] J. M. Tyler and T. G. Sofrin. Axial flow compressor noise studies. *SAE Technical Papers*, 1 1962.
- [37] P. T. Vo and W. Eversman. A method of weighted residuals with trigonometric basis functions for sound transmission in circular ducts. *Journal of Sound and Vibration*, 56:243–250, 1 1978.

- [38] R. YURKOVICH. Attenuation of acoustic modes in circular and annular ducts in the presence of sheared flow. *13th Aerospace Sciences Meeting*, 1 1975.